

Article

COAST-PRO_{SIM}: A Model for Predicting Shoreline Evolution and Assessing the Impacts of Coastal Defence Structures

Pietro Scala , Giorgio Manno , Loredana Claudia Cozar and Giuseppe Ciralo 

Dipartimento di Ingegneria, Università degli Studi di Palermo, 90128 Palermo, Italy; giorgio.manno@unipa.it (G.M.); loredanaclaudia.cozar@community.unipa.it (L.C.C.)

* Correspondence: pietro.scala@unipa.it (P.S.); giuseppe.ciraolo@unipa.it (G.C.)

Abstract: Coastal zones, at the interface between land and sea, face increasing challenges from erosion, sea-level rise, and anthropogenic interventions, necessitating innovative tools for effective management and protection. This study introduces COAST-PRO_{SIM}, a novel numerical model specifically designed to predict shoreline evolution and assess the impacts of coastal defence structures on coastal morphology. Unlike existing models that often face a trade-off between computational efficiency and physical accuracy, COAST-PRO_{SIM} balances these demands by integrating two-dimensional wave propagation routines with advanced shoreline evolution equations. The model evaluates the effects of interventions such as breakwaters and groynes, enabling simulations of shoreline dynamics with reduced computational effort. By using high-resolution input data, COAST-PRO_{SIM} captures the interplay between hydrodynamics, sediment transport, and structural impacts. Tested on real-world case studies along the coasts of San Leone, Porto Empedocle, and Villafranca Tirrena, the model demonstrates its adaptability to diverse coastal environments. The results highlight its potential as a reliable tool for sustainable coastal management, allowing stakeholders to anticipate long-term changes in coastal morphology and design targeted mitigation strategies.

Keywords: coastal erosion; shoreline evolution modelling; coastal defence structures; sediment transport dynamics



Academic Editors: Yunping Yang, Zhiming Chao and Hua Ge

Received: 3 December 2024

Revised: 9 January 2025

Accepted: 16 January 2025

Published: 18 January 2025

Citation: Scala, P.; Manno, G.; Cozar, L.C.; Ciralo, G. COAST-PRO_{SIM}: A Model for Predicting Shoreline Evolution and Assessing the Impacts of Coastal Defence Structures. *Water* **2025**, *17*, 269. <https://doi.org/10.3390/w17020269>

Copyright: © 2025 by the authors. Licensee MDPI, Basel, Switzerland. This article is an open access article distributed under the terms and conditions of the Creative Commons Attribution (CC BY) license (<https://creativecommons.org/licenses/by/4.0/>).

1. Introduction

Coastal zones, representing the dynamic interface between terrestrial and marine environments, hold immense ecological, economic, and social significance [1–3]. These areas are home to diverse ecosystems, such as estuaries, mangroves, and sandy beaches, which provide crucial services, including habitat for marine species, natural coastal defence, and carbon sequestration [4–6]. Simultaneously, coastal zones are focal points of human activity [7,8], hosting dense populations, industries, and tourism-related economies [9,10]. According to estimates by the United Nations, nearly 40% of the global population resides within 100 km of a coastline, underscoring the critical need for sustainable coastal management [11]. However, these regions are increasingly threatened by natural and anthropogenic pressures [12–14], such as accelerated sea-level rise, storm surges, and human interventions like urbanisation and coastal engineering projects [15–18]. These stressors exacerbate erosion, shoreline retreat, and habitat loss, challenging traditional methods of coastal protection and necessitating innovative approaches for effective management [19–22].

The protection and sustainable development of coastal zones require tools and methodologies capable of balancing competing priorities: safeguarding human infrastructure, preserving natural habitats, and accommodating dynamic processes like sediment transport

and wave action [23–26]. Coastal defence structures such as breakwaters, groynes, and seawalls are widely employed to mitigate erosion and protect against flooding [27–30]. While effective in the short term, these structures can significantly alter sediment dynamics and wave energy distribution, leading to unintended consequences such as downdrift erosion and ecosystem disruption [31,32]. Techniques such as beach nourishment, which involves artificially replenishing eroded beaches with sediment, offer more sustainable alternatives but require precise planning and regular maintenance to remain effective [33–35]. The implementation of controlled beach nourishment, achieved through the combined use of nourishment techniques and coastal protection structures, enhances the resilience of the intervention, making it more sustainable over time by synergistically managing sediment transport and wave energy dissipation [36–40]. Understanding the long-term impacts of these interventions is critical for designing resilient coastal protection strategies.

Numerical models have emerged as indispensable tools for predicting shoreline evolution and evaluating the effects of coastal defence structures [32,41–50]. These models simulate the interplay between hydrodynamic forces, sediment transport, and morphological changes, providing valuable insights for decision making. Existing models vary significantly in complexity, ranging from simple one-line (1D) models that solve shoreline changes along a single cross-shore profile to advanced two-dimensional (2D) and three-dimensional (3D) models that provide greater spatial resolution and physical detail [42,48,51–54]. One-line models, based on the Pelnard-Considère (1956) equation, are computationally efficient but may oversimplify coastal dynamics, particularly in environments with significant along-shore variability [55]. On the other hand, more evolved one-line models such as GENESIS, which has been widely used for engineering projects on decades-long scales [56–59], have shown remarkable flexibility and ability to adapt to different scenarios, as documented by [58]. Over more than two decades, GENESIS has been continuously improved to include new functionalities, such as transverse and longitudinal transport, response to coastal structures, and interaction with the beach–dune system. However, its simplified assumptions limit its ability to represent complex interactions between coastal processes, requiring a more integrated approach to address current challenges [60].

Continuing, as highlighted by Splinter and Coco [61], 2D and 3D models, such as Delft3D [52], XBeach [54], and Sbeach [62], offer higher accuracy for short-term or event-scale simulations by capturing lateral variability and detailed hydrodynamic processes. However, these types of models often require significant computational resources, making their application to large-scale or long-term studies challenging [51,63]. Balancing physical realism with computational efficiency remains a persistent challenge, particularly for 3D models where computational demands can limit practical applications to laboratory or very-short-term scenarios [64].

To address these limitations, reduced-complexity physics-based models provide an alternative by simplifying the representation of key processes while retaining the ability to simulate long-term shoreline evolution at broader spatial scales. For instance, equilibrium shoreline models compute changes in response to disequilibrium states, while one-line models integrate gradients in long-shore sediment transport [65]. Despite these advances, traditional reduced-complexity models often oversimplify the effects of human interventions or neglect wave-driven shoreline evolution due to the limited coupling of wave and morphodynamic processes [66]. While recent multi-process reduced-complexity models have attempted to incorporate anthropogenic structures more realistically, challenges remain in accurately representing the spatial variability in wave climate. Moreover, the characteristics of wave breaking, which play a crucial role in wave-driven shoreline evolution, are often either decoupled from morphodynamic processes [67] or overly simplified.

For example, some studies overlook the spatial variability in wave climate within the study area, leading to less accurate representations of coastal dynamics [42,48].

In response to these challenges, we present COAST-PRO_{SIM} (COASTal PROtection SIMulation Model), a novel numerical model specifically designed to predict shoreline evolution and assess the impacts of coastal defence structures with improved computational efficiency and physical accuracy. Compared to established models such as GENESIS or GenCade [68,69], COAST-PRO_{SIM} introduces a more integrated approach that combines wave propagation routines and shoreline evolution calculations, significantly reducing the computational effort. Furthermore, the model is designed to handle a wider range of coastal configurations and operations combined with lower data requirements than traditional process-based models.

COAST-PRO_{SIM} is particularly designed to overcome the limitations of existing models [60] by offering a realistic representation of anthropogenic interventions, such as bypass conditions for groynes and wave diffraction effects behind breakwaters, while maintaining computational efficiency. This balance makes it adaptable to diverse coastal settings and real-world scenarios, enabling its application at regional and centennial scales.

In addition to this first introductory part, this article is organised as follows: Section 2 presents the materials and methods used for the construction of the model and its validation. In Section 3, the results and discussion of the analytical validation and applications to three real-life case studies are presented. Section 4 presents the main conclusions of this work.

2. Materials and Methods

The model requires wave height, direction, and period data as input and simulates the response effects of the coastline in relation to coastal protection works. In particular, the model can simulate the presence of one or more breakwaters or one or more groynes. As an output, the model returns the evolution of the shoreline for each time interval, with limited computational time.

The model is based on two resolution processes: (i) a wave propagation routine to the shoreline using waves propagated up to the near-shore zone as input data and (ii) a multi-process shoreline evolution equation that considers long-shore and cross-shore contributions by accounting for the effects of coastal defence structures on the beach.

In Figure 1, a flowchart of the COAST-PRO_{SIM} model is presented which highlights the steps that make up the execution and operational framework of the model.

The model does not compute propagation from offshore to the sub-coast; in fact, the data to be provided as input to the model were obtained through the near-shore hybrid downscaling technique [70] which exploits SWAN propagation of spectral wave data. In order to exploit this method, marine magnitude data of significant wave height H_s , wave direction with respect to the shoreline θ , and peak period T_p downloaded from the CMEMS database or nowadays CMS (Copernicus Marine Service) were used. The results were then propagated from COAST-PRO_{SIM} to the shoreline to solve the shoreline evolution equation.

The COAST-PRO_{SIM} model therefore requires a set of input parameters that are fundamental for the accurate simulation of the shoreline evolution. Among these, the time series of wave motion characteristics output to the downscaling play a central role. These parameters must be provided as time series with hourly resolution, thus determining the simulation period: for example, twenty years of hourly data allow the simulation of a coastal evolution over an equivalent period. A second set of parameters concerns the initial morphological characteristics of the domain. The position of the shoreline is represented by a vector describing its initial configuration along the coastal domain, while a further vector indicates the slopes of the transects orthogonal to the shoreline. These slopes are calculated between the initial position of the shoreline and the closure depth, assuming that, in the

propagation zone, the bathymetric lines are approximately parallel to the shoreline [71]. This hypothesis, supported by Snell's law (see Section 2.2.2), links morphological changes to wave propagation, with the translation of the coastal profile indirectly represented by the variable orientation of the shoreline over time. The median value of the sediment diameter (D_{50}), the closure depth (h_c) value (which is calculated by the model once the H_s time series data have been entered), and a vector of the berm height for each transect are added to these parameters. Moreover, the hypothesis of the model is that sediment transport along the coast occurs up to the closure depth and no further.

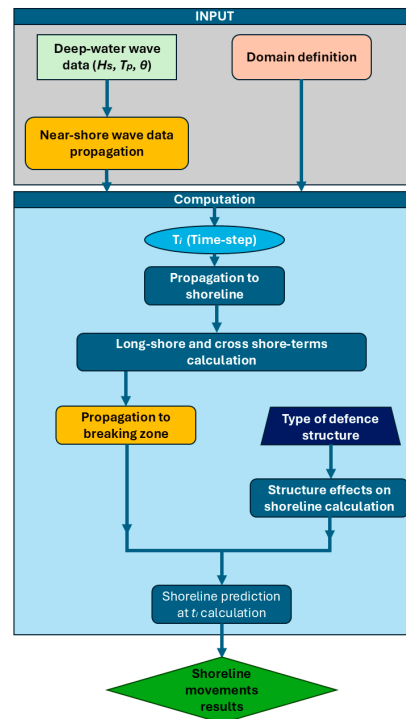


Figure 1. Flowchart of the COAST-PROSIM operations.

For each structure to be simulated, it is necessary to specify the type and the position with respect to the shoreline, as well as the geometric characteristics such as length, height, and, in the case of multiple configurations, the distance between the structures. Finally, it is necessary to indicate the values of solid flow entering or leaving the domain that will represent the rates of retreat or growth of the shoreline not due to wave–beach interaction (e.g., sediment sampling or inlets from basins) which is added or subtracted homogeneously over the entire domain.

The model offers flexibility in the output of results, allowing us to choose between hourly, daily, or monthly time resolutions. This feature makes the model suitable for simulations ranging from short-term studies to coastal evolution scenarios over periods of several decades.

COAST-PRO_{SIM} utilises a temporal discretisation based on explicit methods that balance accuracy and computational stability, ensuring rapid convergence. The staggered spatial grid is defined on a domain divided by transects, allowing the integration of cross-shore and long-shore processes. To solve the governing equations, the model adopts an explicit forward scheme for time and a finite difference scheme for spatial discretisation.

The stability of the model is ensured by respecting the Courant–Friedrichs–Lewy (CFL) criterion, calculated as in Equation (1).

$$C = \frac{\Delta t}{h_c \Delta x^2} \cdot Q \leq 1 \quad (1)$$

where Δt represents the time step, Δx is the spatial resolution between transects, and Q is the solid transport rate. This approach reduces the calculation time while maintaining the accuracy required for engineering analysis.

The numerical stability of the equation is guaranteed as suggested by [42].

2.1. Solving Equation

The evolution equation of the multi-process coastline of COAST-PRO_{SIM} (Equation (2)) considers the two components of long-shore and cross-shore coastal sediment transport.

$$\frac{\partial Y_U}{\partial t} = \frac{\partial Y_{U1}}{\partial t} \pm \frac{\partial Y_{U2}}{\partial t} \pm \rho' \quad (2)$$

Y_U represents the shoreline location due to total transport (m); the derivative represents its temporal variation that depends on parameters that also vary spatially. Y_{U1} represents the shoreline location due to long-shore transport (m). Y_{U2} represents the shoreline location due to cross-shore transport (m). t is the time (i.e., days or hours), and ρ' represents the terms of loss and gain of sediment to and from the outside expressed in m/s to be consistent with the units in Equation (2). The input data are given as sediment discharge in m^3/s at the outlet or inlet (e.g., sediment discharge entering a river mouth), to obtain an advance or retreat velocity consistent with the required units. The model then divides the discharge by the cross-sectional area of the analysis domain. This area is defined as the surface perpendicular to the shoreline, extending from the shoreline to the closure depth for each transect. The cross-sectional area can then be expressed as the sum of the product of the individual transect length, L_x , and the closure depth.

2.2. Near-Shore Propagation Modelling

The main phenomena associated with wave motion during its propagation and simulated by the model are (i) shoaling, (ii) refraction, and (iii) diffraction, breaking, and reflection.

2.2.1. Shoaling Modelling Approach

Shoaling consists of an increase in the steepness of the wave due to the change in the depth of the seabed as it propagates from offshore towards the coast. And since the principle of the conservation of energy applies, a change in the depth of the seabed corresponds to a change in the wave height [72]. The proposed model considers linear shoaling, which is a simplified approach to describe this phenomenon. In linear shoaling, it is assumed that the wave energy is conserved and evenly distributed as the wave approaches the shore, resulting in a gradual and predictable increase in wave height in proportion to the decrease in water depth.

According to Bosboom and Stive [73], the steeped wave height can be deduced from Equation (3).

$$H = H_s K_s \quad (3)$$

where K_s is the shoaling coefficient expressed as in Equation (4).

$$K_s = \sqrt{(2\cosh^2(kh)) / (2kh + \sinh(2kh))} \quad (4)$$

Here, k is the wave number (m^{-1}) equal to $\frac{2\pi}{L}$ with L wavelength (m).

2.2.2. Refraction Modelling Approach

Refraction occurs when the wave rays propagating towards the shore form a non-zero angle perpendicular to the bathymetrics (i.e., they have an oblique attack). This causes the wavefronts to rotate as they move from deep to shallow water and causes them to lie

parallel to the bathymetrics and the shoreline (according to the basic assumption of the model discussed in Section 2.2.2). This effect occurs because in the same wave front there are different depths and therefore different celerities, less as the seabed interacts with the wave [72].

To study refraction, COAST-PRO_{SIM} uses the simplified one-dimensional Snell treatment given in Equation (5) and the principle of the conservation of wave energy along the wave rays (the lines along which waves propagate).

$$\frac{\sin\theta_b}{L_b} = \frac{\sin\theta_0}{L_0} \quad (5)$$

in which θ_b and L_b are the angle and wave height at the break (m), while θ_0 and L_0 are the angle and wave height offshore in deep water (m).

The angle of wave attack is calculated in order to determine the angle of incidence of the waves along each transect, taking into account the spatial variation in the orientation of the coastline (assuming the bathymetric lines are parallel to the coastline). This angular rotation is updated at each time step. In the case of wave propagation, the orientation of the variable shoreline is used to calculate the angle of incidence, which in turn affects the direction of wave propagation and the distribution of energy along the shoreline. The model thus ensures that the angle of attack is updated at each time step.

2.2.3. Diffraction Modelling Approach

Diffraction is a phenomenon that occurs when sea waves encounter an obstacle, such as a reef, cliff, island, or man-made structure. This obstacle causes a change in the direction and shape of the waves. Diffraction manifests itself as the ability of waves to bypass the obstacle and propagate laterally behind it, creating new wave fronts. When a wave crosses an obstacle, part of the wave energy is reflected, while another portion passes through the obstacle if it is partially permeable. In addition, some of the energy is diffracted, redistributing itself around the obstacle and curving the waves behind it. This phenomenon changes the wave regime behind the obstacle, making them weaker and less high than the direct waves, creating an area of relative calm. The diffracted waves form new fronts that can interfere with each other, leading to changes in the wave pattern and redistributing energy along an arc behind the obstacle. This can reduce erosion in some coastal areas and increase it in others.

Understanding diffraction is fundamental to designing harbours, jetties, breakwaters, and other coastal structures. These structures must be correctly positioned and sized to minimise coastal erosion and protect beaches. Furthermore, diffraction affects the distribution of sediments along the coast and thus the morphology of the beach. Knowing how waves spread behind an obstacle helps predict areas of accumulation or erosion, contributing to the protection of coastal infrastructure from wave force, especially in areas where wave energy can be reduced through natural or artificial obstacles.

COAST-PRO_{SIM} uses empirical Kamphius diffraction laws [74,75] to correct for breaking properties in the presence of detached groynes and breakwaters. It also considers morphological changes influenced by wave propagation, which is controlled by the orientation of the shoreline, which varies over time and influences refraction according to Snell's law in Equation (6). Consequently, the translation of the profile is indirectly explained by the evolution of the shoreline orientation.

$$H_{s(b)} = H_s \sqrt{\frac{\cos(\theta_0)}{\cos(\theta_b)}} \sqrt{\frac{C_g}{\sqrt{g} h_b}} \quad (6)$$

in which $H_{s(b)}$ is the transformed significant wave height (m); H_s is the significant wave height before transformation (m); θ_b is the wave angle at the break obtained from Snell's Law in 5; θ_0 is the wave angle offshore in deep water; and C_g is the group celerity (m/s) calculated as in Equation (7):

$$C_g = 0.5 C \left(1 + \frac{2kh}{\sinh(2kh)} \right) \quad (7)$$

Here, C is the celerity of the wave (m/s); h is the local depth (m).

The formula for wave height diffraction, proposed by Kamphuis [75], is given by Equation (8):

$$H'_{s(b)} = \sigma_d H_{s(b)} \quad (8)$$

where the diffraction coefficient σ_d is determined by the angle of attack θ and can be calculated using two different formulations depending on the value of θ , in particular, the formulation for $-90 < \theta < 0$ in Equation (9) and that for $0 < \theta < \theta_r$ in Equation (10) where θ_r is the maximum angle of diffraction:

$$\sigma_d = 0.71 - 0.0093 \theta + 0.000025\theta^2 \quad (9)$$

$$\sigma_d = 0.71 + 0.29 \left[\sin \left(90 \frac{\theta}{\theta_r} \right) \right] \quad (10)$$

Using the above-reported equations, it is possible to calculate the height of the diffracted wave taking into account the angle of attack of the waves. This helps to predict the effectiveness of coastal defence works in reducing wave energy and protecting the coast from erosion.

2.2.4. Breaking Modelling Approach

Breaking occurs when the waves, due to shoaling or refraction, reach a critical height with a certain steepness, destabilise, and lose their shape by breaking, with a more or less violent dissipation of energy, accompanied by strong turbulence and possible foam formation. Breaking can have different effects depending on the slope of the seabed and the characteristics of the wave.

In COAST-PRO_{SIM}, a constant depth-induced (h) breaking index of 0.78 was assumed according to Laitone's criterion [72,76] in which the wave stabilises after shoaling and begins to break (breaking condition in Equation (11)).

$$H'_{s(b)} = 0.78 h \quad (11)$$

2.2.5. Reflection Modelling Approach

Wave reflection occurs when a wave train encounters an obstacle, such as a vertical wall, an inclined surface, or a submerged barrier, with the degree of reflection depending on the geometry, material properties, and surface roughness of the obstacle. In this process, the waves reflect back on themselves with a modest loss of energy. When the period of the waves is regular, a standing wave system can be formed.

This process not only affects the morphology of the seabed but also the distribution of sediments. Reflection can increase erosion near the base of the obstacle, as refracted wave energy is concentrated in this area, thus causing an increase in wave height and pressure and causing resonances in closed basins. In COAST-PRO_{SIM}, the effects of wave reflection were considered negligible in the presence of coastal structures that favour refraction. Furthermore, the model is designed to simulate shoreline evolution and sediment transport on long time scales, where reflection has little impact compared to wave propagation and

transport processes. While recognising the importance of reflection, it is considered a secondary effect in the context of long-term simulations, where the influence of sediment transport processes is preponderant [77,78].

2.3. Solid Transport Module

Normally, a beach is made up of sediments of various grain sizes, from the finest sands to gravel. These are mostly found in different positions: the coarser sediments typically have a diameter of more than 2 mm and are found close to the swash zone, in the steepest part of the profile; the medium and fine sands, with diameters varying between 0.063 mm and 2 mm, are found as one moves in the offshore direction, where they are distributed according to the long-shore current and cross-shore dynamics [75].

Shores are affected by a circulatory system determined by currents that can be “coastal” or “littoral”. Coastal currents are those occurring offshore of the breaker zone, typically driven by larger forces such as wind and tide. Littoral currents, on the other hand, are wave-driven currents located in the surf zone, which the model simulates.

2.3.1. Long-Shore Component Modelling

Estimating the usual coastal transport is very complex, as it depends on many different factors, such as the wave characteristics, type of breaking, sediment characteristics, slope of the beach, and roughness of the seabed.

Two different approaches can be used to obtain estimates of sediment transport: the total law or the distribution law. Only the first approach has been dealt with here, which refers to a methodology that estimates the total sediment transport along the coast, without distinguishing between the different contributions of the individual transport components, i.e., it focuses on the entire amount of sediment moved by wave motion and currents, considering the phenomenon in a global way.

The total approach is typical of the CERC-formula [79], which estimates the total transport in the breakwater zone and establishes a direct dependence between the energy flux associated with a wave in a direction parallel to the coast and the sediment transport in that direction (Shore Protection Manual, 1984—<https://luk.staff.ugm.ac.id/USACE/USACE-ShoreProtectionManual1.pdf>, accessed on 28 October 2024).

Although the CERC formula is a frequently used method, it has some limitations that can lead to under- or overestimates of sediment transport. The CERC formula assumes that sediment transport is dominated by waves breaking obliquely to the coastline with a constant direction of transport along the coast, whereas in reality, the direction of transport may vary depending on the local and temporal conditions of waves and currents. The constant K in the formula, which represents the relationship between wave energy and sediment transport, is empirical and can vary greatly depending on local conditions. The accurate determination of this value requires site-specific data and can be difficult to generalise. The formula is based on the wave height at the breaking point H_b , but offshore waves can vary considerably in height and wavelength, affecting sediment transport in complex ways that the formula does not capture. Another limitation is the use of the angle of incidence of the waves φ_b with respect to the coastline. This angle can change rapidly with changes in meteorological and oceanographic conditions, making it difficult to accurately estimate sediment transport over time. The formula may underestimate sediment transport in areas where coastal currents and tides play a dominant role or in situations where waves have a significant impact outside the breaking zone. On the other hand, it may overestimate transport in conditions where waves are less energetic than expected or where sediments are less mobile, e.g., coarser sediments or cohesive conditions between sediments [80–83]. Finally, the formula does not capture non-linearities and

complex interactions between waves, currents, and sediments over time (such as breaker type and grain size [84,85]), limiting its accuracy in long-term predictions. For all these reasons and in order to build a model that does not necessarily require the calibration of the coefficient K , we decided to use another long-shore transport empirical formulation.

In fact, the Kamphuis [74] formula is an empirical method developed to estimate *long-shore* transport and considers various factors influencing sediment transport by providing a more accurate estimate of the volume of sediment transported per unit time. The formula is expressed by Equation (12):

$$Q = 7.3 H_b^4 T_p^{1.5} s^{0.75} \left(\frac{D_{50}}{1000} \right)^{-0.25} (\sin(2(\varphi_b)))^{0.6} \quad (12)$$

in which Q is the sediment flow rate (m^3/s); H_b is the wave height at the breaking point (m). This term is raised to the fourth power, indicating that sediment transport is highly sensitive to wave height. Higher waves result in significantly greater sediment transport; T_p is the peak wave period (s). This term suggests that sediment transport increases as the period of the waves increases. Waves with longer periods tend to have more energy and thus greater capacity to transport sediment; s is the slope of the beach. The beach slope is elevated to the power of 0.75, indicating that beaches with steeper slopes favour greater sediment transport; D_{50} is the median diameter of the sediment granules (μm). This term shows that sediments with smaller granules (smaller diameter) tend to be transported more easily than those with larger granules. Finally, φ_b is the angle of incidence of the waves with respect to the coastline at the breaking point (degrees). This term indicates that the angle of incidence of waves has a significant effect on sediment transport. Waves that strike the coast at an oblique angle (as opposed to perpendicular) tend to transport more sediment along the coast.

Equation (12) represents an important evolution in coastal sediment transport estimation tools, providing a more detailed and specific estimate than the CERC formulation [65].

This COAST-PRO_{SIM} is based on the mass continuity equation and a sediment transport equation along the coastline. Under the simplifying assumptions of a moderate shoreline gradient and small wave angle with respect to the shoreline, the first analytical solutions of the one-line model involve the concentration of the two equations into a single equation of diffusive type, as shown in Equation (13) [71].

$$Q \frac{\partial Y_{U1}}{\partial t} = \varepsilon \frac{\partial^2 Y}{\partial x^2} \quad (13)$$

in which Y_{U1} represents the location due to long-shore transport (m); x is the distance on an X axis parallel to the coastline (m); y is the position of the coastline on a vertical Y axis at X (m); t is time (days); and ε is the diffusion coefficient (m^2/s) given by the expression in Equation (14).

$$\varepsilon = \frac{2Q}{d_b + h_c} \quad (14)$$

in which Q is the long-shore transport (m^3/s) estimated with the expression in Equation (12); d_b is the height of the berm (m); and h_c is the closure depth (m) calculated using Hallermeier's formula.

2.3.2. Cross-Shore Component Modelling

The cross-shore sediment transport component is given by Equation (15) which is derived from empirical and theoretical modelling studies of sediment transport in coastal environments [79]. These studies often combine field observations, laboratory experiments, and mathematical modelling to derive relationships that describe how sediments are

transported by waves and currents. Equation (15) is particularly useful for predicting how sediments move during storm events, tides, and other hydrodynamic forcing.

$$Y_{U2} = -W \left(\frac{0.106 H'_{s(b)}}{d_b + h_b} \right) \quad (15)$$

Y_{U2} represents the location due to cross-shore sediment transport (m); 0.106 is a coefficient derived from empirical adjustments based on data observed under different coastal conditions; $H'_{s(b)}$ represents the significant wave height at the breaking point (m); and h_b represents the depth at which the breaking occurs (m). Note that all these terms depend on time and space.

W (Appendix B) represents the width of the surf zone, i.e., the area where wave breaking occurs (m). Please refer to Appendix B for more information about Equation (15) terms and calculation.

2.3.3. Effects of Structures Modelling

A tombolo (and with the same mechanism a salient) is formed when a barrier, such as a breakwater or groyne, alters the natural movement of waves and sediment along the coast. Normally, sediments, such as sand and gravel, are transported along the coast by waves and currents, but when a barrier is placed in the sea, it interrupts this natural flow. The barrier acts as an obstacle that reduces the energy of the waves hitting the coast behind, thus decreasing the ability of the waves to transport sediment. As a result, sediment begins to settle in the area behind the barrier itself. The sand transported by the currents accumulates on the upstream side of the barrier, beginning to form a salient that, as it gradually increases, may become completely connected to the barrier, creating a land connection between the coast and the structure (tombolo).

Once the tombolo is formed, it tends to stabilise, as the waves behind the barrier are weaker and continue to deposit sediment instead of eroding it. However, the stability of the tombolo depends on the size and position of the barrier, as well as wave and sediment transport conditions.

COAST-PRO_{SIM} can model and visualise the salient and tombolo formation at T-shaped groynes and detached breakwaters. It is essential, to this end, to impose that the beach can reach the structure but without crossing it or being carried beyond it. To this end, the model dictates that when a calculation cell (area between two consecutive transects) contacts the structure, the transport discharge in that cell is adjusted to allow excess sediment to remain in the ascending cells. The procedure must preserve the sediment volume and preserve the direction of its transport. Specifically, in cell i th + 1, a tombolo was formed at a previous time step. In the adjacent cell i th, by allowing the inflow from cell i th – 1, the shoreline would advance beyond the barrier, which is not permitted. Therefore, the initially calculated inflow velocity must be corrected so that the coastline advances to the barrier but not beyond it.

The same reasoning applies in longitude for the groynes. When the maximum advance is reached at the back of the groyne, the advance is stopped. The excess sediment is divided between the sediment that bypasses the structure and the excess to the adjacent cell, which then goes into accretion.

2.4. Validation Methods

The model COAST-PRO_{SIM} is a one-line model that solves the Equation (2). in which it estimates the shoreline location due to total sediment transport as the sum of the location terms due to long-shore and cross-shore transport, as well as any inputs and outputs to

and from the outside. In particular, the application of the model in this work takes place within a physiographic unit, whereby exchanges with the outside can be considered zero.

For the validation of the model, a preliminary analysis of the model was carried out on synthetic cases of linear shoreline, oriented northwards with a normal at 0° N, under conditions of constant and synthetic meteorological and sea forcing, simulating the variation in the beach line with the effect of the presence of the following:

- A semi-permeable detached breakwater;
- A semi-permeable groyne.

We would like to specify that, while the first analytical solutions in the literature dealt with the case of groynes and impermeable barriers of infinite length, the present one aims to describe a condition that more closely reflects the actual conditions that allow the transport of sediment through and around such works, which are therefore semi-permeable and of finite length.

2.4.1. Validation Metrics

For the validation of the COAST-PROSIM model and its ability to predict the coastline in the presence of protective works, reference is made to established methodologies in the literature. The results obtained are compared using specific validation metrics. The metrics chosen for this analysis are the correlation coefficient, CC; the mean error, BIAS; the mean square error, RMSE; the normalised mean square error, NMSE; and the coefficient of determination R^2 .

For more information on the equations and the description of each validation indicator, please refer to Appendix C.

2.4.2. Semi-Permeable Detached Breakwater Validation

For the validation of COAST-PRO_{SIM} and its ability to predict the coastline due to the effect of a semi-permeable detached breakwater, reference is made to Silvester and Hsu's methodology proposed in 1997 [80] by comparing the results obtained through the use of the chosen validation metrics (Section 2.4.1).

The method proposed by Silvester and Hsu, also known as the parabolic bay shape method, is used to predict the evolution of the shoreline following the insertion of a breakwater. This method is based on the geometric configuration of the bay that is formed as a result of wave interaction with the barrier [80]. Silvester and Hsu's model was selected as the reference for comparison because of its well-established application in the context of coastal defence structures [81].

Considering that L_s represents the length of the breakwater barrier (m), X represents the distance of the shoreline from the horizontal axis of the barrier (m), R_0 represents the length of the parabolic bay (m), and θ_{SH} is the angle of attack of the wave on the breakwater, the formula for predicting the shoreline R_0/L_s is given by Equation (16).

$$\frac{R_0}{L_s} = C_0 + C_1 \left(\frac{\beta}{\theta_{SH}} \right) + C_2 \left(\frac{\beta}{\theta_{SH}} \right)^2 \quad (16)$$

in which β is the angle between the wave crest at the point of diffraction and the control line, and C_0 , C_1 and C_2 are coefficients that depend on the angle β .

The relationship between R_0/L_s and L_s/X is expressed by Equation (17).

$$\frac{R_0}{L_s} = 0.1737 + \frac{1.683}{L_s/X} \quad (17)$$

This equation helps determine the specific shape of the bay based on the geometric parameters of the configuration. In particular, for an angle $\beta = 10^\circ$ and for the configuration

with a single breakwater on a straight beach, the coefficients take the values $C_0 = 0$; $C_1 = 1.32$; and $C_2 = -0.33$.

2.4.3. Semi-Permeable Groyne Validation

For the validation of COAST-PRO_{SIM} and its ability to predict the coastline influenced by a semi-permeable shoreline, we refer to the studies by A. Valsamidis and D. E. Reeve [71], in which analytical solutions are applied with satisfactory results in simple situations, such as a single permeable groyne or for a compartment of groynes.

The method proposed by Valsamidis and Reeve consists of combining the semi-analytical solution for predicting the evolution of the shoreline in the vicinity of a single groove [82] with that derived by Zacharioudaki and Reeve [83] for a complex of groynes, using appropriate boundary conditions so that a model can be developed that is suitable for describing a field of several groynes positioned in succession.

Concerning the semi-analytical solution for the prediction of shoreline evolution in the vicinity of a single groyne [82], a Fourier cosine transform is used to develop the solution to the diffusive equation (Equation (14)). This solution is given by the sum of the following three terms in Equation (18).

$$Y^G = Y_1^G + Y_2^G + Y_3^G \quad (18)$$

in which Y^G is the position of the coastline. For more information on the methodology and the related equations used to validate the groyne case, please refer to Appendix D.

For both validations (breakwater and groyne), the input data shown in Table 1 were used.

Table 1. Validation input data.

Input Data	Values
Groyne length (Y) [m].	15
Mean wave height at breaking (H _b) [m].	1
Beach slope (s) [-]	0.01
Closing depth (h _c) [m].	7.5
Significant sediment diameter (D ₅₀) [mm].	0.5
Mean breaking angle (ab) [°].	10
Berm height (db) [m].	1
Mean peak period (T _p) [s].	6

2.5. Validation Study Areas

To assess the reliability of COAST-PRO_{SIM} in predicting the evolution of the coastline in the presence of coastal works, such as barriers and groynes, three pilot sites characterised by different environmental conditions were selected: San Leone, Porto Empedocle, and Villafranca Tirrena.

These locations were selected for their geographical relevance and the diversity of coastal conditions present, which allow the model to be tested in varied and complex scenarios. San Leone is a seaside resort characterised by high coastal dynamics and significant erosion phenomena. The presence of anthropogenic structures makes this site particularly interesting for assessing the model's effectiveness in predicting interactions between infrastructure and coastlines. Porto Empedocle, known for its commercial port, represents a different context in which port works and human activities greatly influence coastal morphology. Studying this area makes it possible to verify the model's ability to adapt to an environment strongly modified by human activities and to predict the evolution of the coastline in the presence of intense port activities. Finally, Villafranca Tirrena offers an opportunity for analysis in a natural coastal context with a lesser presence of artificial structures. This location is characterised by erosional and depositional processes typical of

sandy coasts, providing a test bed for the model under more natural conditions and less influenced by human intervention.

Model results in the last configuration in December 2023 were compared with observations from satellite images acquired at different times temporally close to the simulation end date using the automatised shoreline detection method presented by, in particular, the Bing Satellite in October 2023; ESRI Satellite in July 2023; Google Satellite in May 2023; and Google Satellite in March 2024. The shorelines were detected using the methodology Presented by Scala et al. [84]. The obtained shorelines (for each case study area) were processed using the CDA plugin [22] in order to conduct a transect-based comparison between the detected shorelines and COAST-PRO_{SIM} results.

The comparative analysis of these three case studies made it possible to assess the reliability and versatility of the forecasting model developed, providing valuable indications for its use in real contexts and for sustainable coastal management.

The first application site is San Leone beach, located on the southern coast of Sicily in the municipality of Agrigento, which features a low sandy shoreline interrupted by rocky outcrops and small promontories. The area is characterised by fine sediments, with coarser materials near river mouths, and small hills composed of robust lithologies such as limestone. Since the 1970s, significant human interventions have disrupted coastal dynamics, leading to shoreline erosion, particularly pronounced during winter. Coastal defence structures, including groynes, breakwaters, retaining walls, and artificial nourishment, have altered sediment transport and deposition. The marina of San Leone has further influenced local currents, exacerbating these changes.

Porto Empedocle, also situated along the southern Sicilian coast, shares similar geomorphological features with San Leone. Here, the COAST-PRO_{SIM} model was applied to predict shoreline changes after the construction of a harbour, whose inner arm functions as a long groyne. The results were validated with satellite imagery, highlighting the harbour's significant impact on sediment flow and coastal dynamics.

Villafranca Tirrena beach, on the northeastern coast near Messina, consists of fine golden sands with sporadic gravel and pebbles near river mouths. The area is also notable for its coastal dunes, which provide protection against storm surges. However, the beach has experienced consistent erosion due to reduced sediment inputs, the regulation of local torrents, the construction of ports and coastal defences, and urban expansion. Despite the presence of 14 breakwaters, the beach has narrowed significantly, with some sections disappearing altogether. Coastal roads and infrastructure close to the shore, along with tourist facilities, have further complicated erosion and coastal management efforts.

Wave Data

For the three case studies under consideration, namely San Leone, Porto Empedocle, and Villafranca, reanalysis data obtained free of charge through the Copernicus Marine Environment Monitoring Service (CMEMS or Copernicus Marine Service CMS) portal (<https://data.marine.copernicus.eu/products>—accessed on 28 October 2024) were used to characterise the meteorological climate. These data are hourly averages of the following: significant wave height [m]; wave direction of significant height [°]; and wave period at maximum spectral density [s]. The acquired data, calculated on an hourly basis, cover a time interval of 29 1/2 years, from 1 January 1993 at 00:00 to 30 July 2022 at 23:00.

For each of the three case studies, the wave rose (Figure 2) is shown for the meteomarine characterisation. In each wave rose, the sectors are described by a length indicating the number of elements within specific percentage thresholds and a colour gradation representing the intensity of the variable—i.e., the significant wave height. The distribution of the waves is a function of the frequency of occurrence (%), represented by concentric circles.

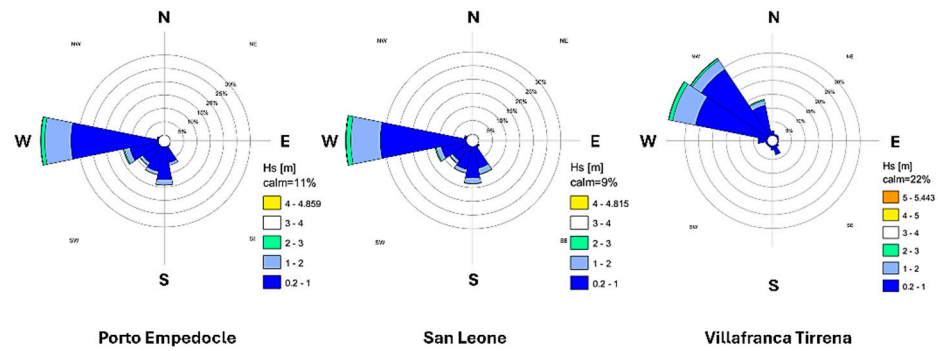


Figure 2. Wave roses for the three application study sites.

The analysis of the wave roses for the three sites shows that the most frequent and intense waves come from quadrant IV, particularly from the west and northwest (especially for Villafranca). In all cases, the highest value of significant height is recorded in the direction of approximately 270–290° N, with a frequency of over 30%. The calm condition, associated with significant heights of less than 0.2 m, occurs with an occurrence rate of about 11%, 9%, and 22% of the total for San Leone, Porto Empedocle, and Villafranca Tirrena, respectively.

The wave height, direction, and period data described above were subsequently used as input for the near-shore hybrid downscaling [70], the results of which were used as input for the COAST-PRO_{SIM} model.

3. Results

In this section, the results of the analytical and real case studies’ validation are presented.

3.1. Breakwater Analytical Validation Result

In the evaluation of predictive models, the use of validation metrics is crucial to quantify the accuracy of the predictions of one model compared to another. Such metrics not only provide a measure of the error committed by the model but also allow one to compare the effectiveness of different models or approaches, as in the case of the comparison between the proposed COAST-PRO_{SIM} and the Silvester–Hsu technique for shoreline prediction.

In the outline of this validation, *L* is the length of the barrier (m), and *S* is the distance of the shoreline from the horizontal axis of the barrier (m).

Simulations were carried out for 33 configurations differing in *S* length but maintaining a constant *L* value of 100 m and considering the shoreline discretisation based on 600 transects with 1 m resolution spacing. The configurations are shown in Table 2.

Table 2. Values used for simulation with barrier.

Conf. [n°]	L [m]	S [m]	Conf. [n°]	L [m]	S [m]	Conf. [n°]	L [m]	S [m]
1	100	175	12	100	120	23	100	65
2	100	170	13	100	115	24	100	60
3	100	165	14	100	110	25	100	55
4	100	160	15	100	105	26	100	50
5	100	155	16	100	100	27	100	45
6	100	150	17	100	95	28	100	40
7	100	145	18	100	90	29	100	35
8	100	140	19	100	85	30	100	30
9	100	135	20	100	80	31	100	25
10	100	130	21	100	75	32	100	20
11	100	125	22	100	70	33	100	15

Figure 3 shows the comparison between the results obtained using COAST-PRO_{SIM}, shown as blue asterisks, and those obtained using the method proposed by Silvester and Hsu [80], used in this work as a reference method, shown as a red dashed line. An initial graphical analysis shows a high degree of closeness between the values of the two methods (consistent fit). For analytical comparison, the relative values of the chosen validation metrics are also shown (Table in Figure 3).

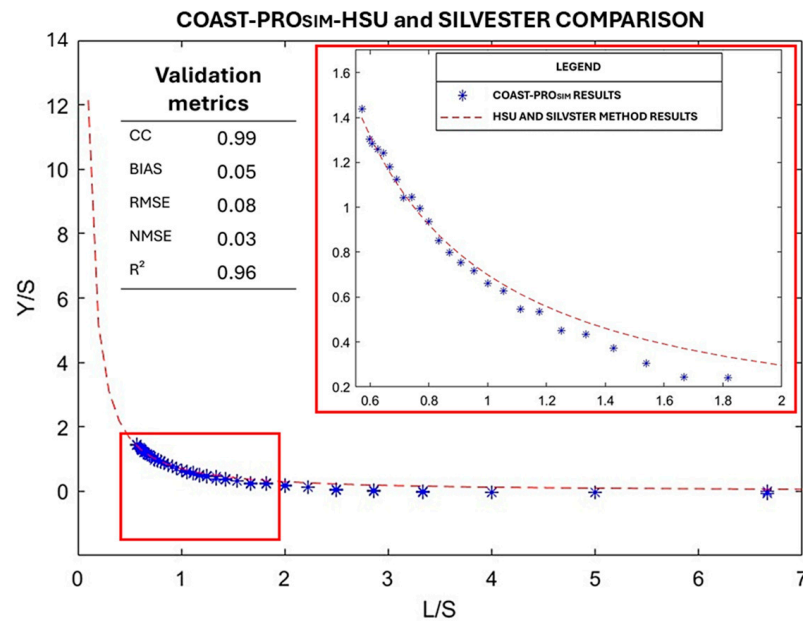


Figure 3. Comparison of the results obtained with COAST-PRO_{SIM} and the Silvester and Hsu method with relative values of the validation metrics: correlation coefficient, BIAS, RMSE, NMSE, and coefficient of determination R^2 .

The values obtained in the validation metrics table indicate that COAST-PRO_{SIM} is suitable for the prediction of the shoreline following the insertion of a breakwater. In particular, the correlation coefficient is very close to a value of 1, the BIAS does not show large overestimates or underestimates, the RMSE value is low, suggesting high accuracy, the NMSE value is very close to a value of 0, and finally, the coefficient of determination R^2 is high.

After comparing the validation metrics, simulations were carried out to predict the shoreline location by solving Equation (2) for a time span of 20 years, with a daily simulation.

Of the thirty-three configurations shown in Table 3, six representatives were chosen and are shown in Table 3. The graphical results of the shoreline location with the final configuration on simulation day 7201 are shown in Figure 4.

Table 3. Configurations shown graphically.

Conf. [n°] and Subplot ID	L [m]	S [m]
1-A	100	175
15-B	100	105
20-C	100	80
27-D	100	45
30-E	100	30
33-F	100	15

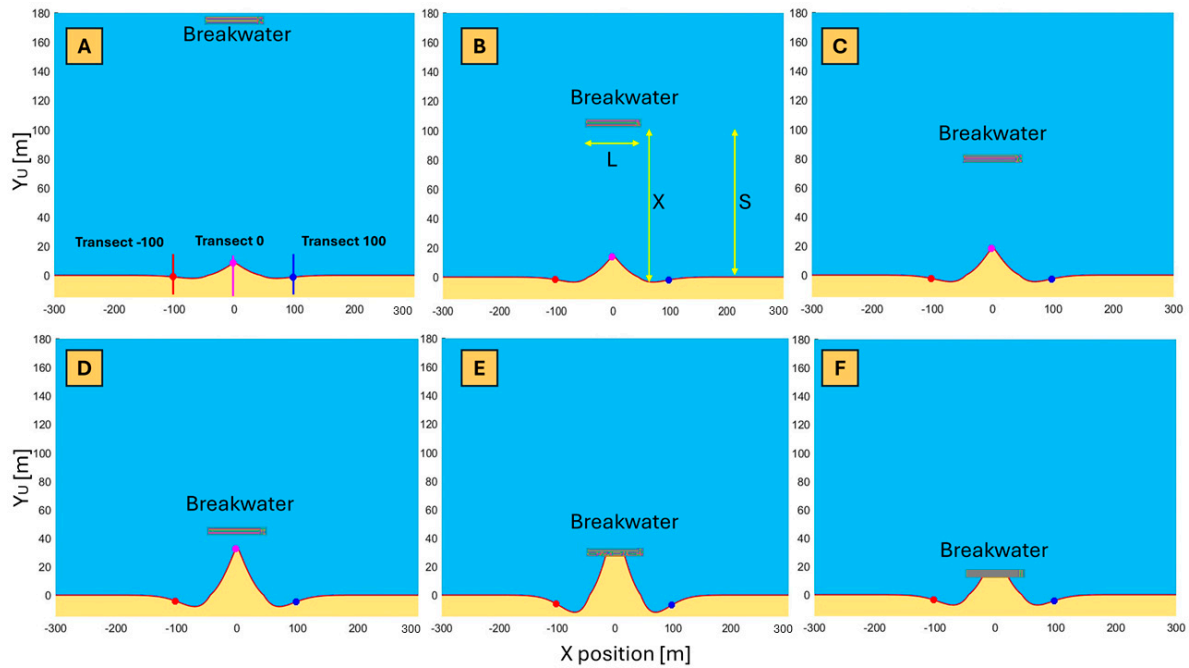


Figure 4. Trend of Y_u on simulation day 7201 for the six configurations (subplot from (A–F)) selected in Table 3 considering a 20-year simulation. Red, magenta and blue transect represent respectively 100, 0 and +100 m transect dots. Points depict the location of selected transects in all subplots.

In Figure 4, it is possible to observe the position of three selected transects, named Transect –100, Transect 0, and Transect 100 on simulation day 7201, the time when the structure is fully operational, for the six chosen configurations. Note that in the graph of configuration 1, the three transects are represented as follows: Transect –100 in red; Transect 0 in magenta; and Transect 100 in blue.

This colour coding is also kept constant in the plot of subsequent configurations. The barrier, highlighted in grey, has a constant length of 100 m.

The analysis of the results clearly shows how the presence of the barrier constitutes an obstacle that induces a dissipation of wave energy and, consequently, a reduction in the sediment transport capacity along the coast. The sediment, deprived of its kinetic energy, tends to settle upstream of the structure, giving rise to a salient that, as the simulation progresses, gradually increases until it joins the barrier itself, forming a tombolo. This phenomenon can be observed from configuration 30 onwards. This occurs because, as mentioned in the presentation phase, COAST-PRO_{SIM} is able to model and visualise the formation of the salient and the tombolo at the structure, taking into account that the sediments can only reach the structure without crossing it or being transported beyond it.

The quantitative analysis of the results indicates that the distance from the shoreline significantly influences the morphology of the tombolo. In particular, for distances greater than 40 m, the barrier is too far from the shoreline to affect the formation of a complete tombolo. On the contrary, for distances of less than 30 m, as in the case of configuration 30, a clear morphological evolution is observed with the formation of a well-defined tombolo.

Figure 5 represents the temporal evolution of the shoreline position (Y_u) in three transects (–100 m, 0 m, and 100 m) in two breakwater positioning configurations. In subplot A, related to configuration 1, the breakwater is located 175 m from the coast, while in subplot B, related to configuration 33, it is located much closer, 15 m from the coast. The dynamics of the system are analysed over a time span of approximately 20 years (7000 days), highlighting the differential effects of the two configurations on coastal sediment accumulation and erosion.

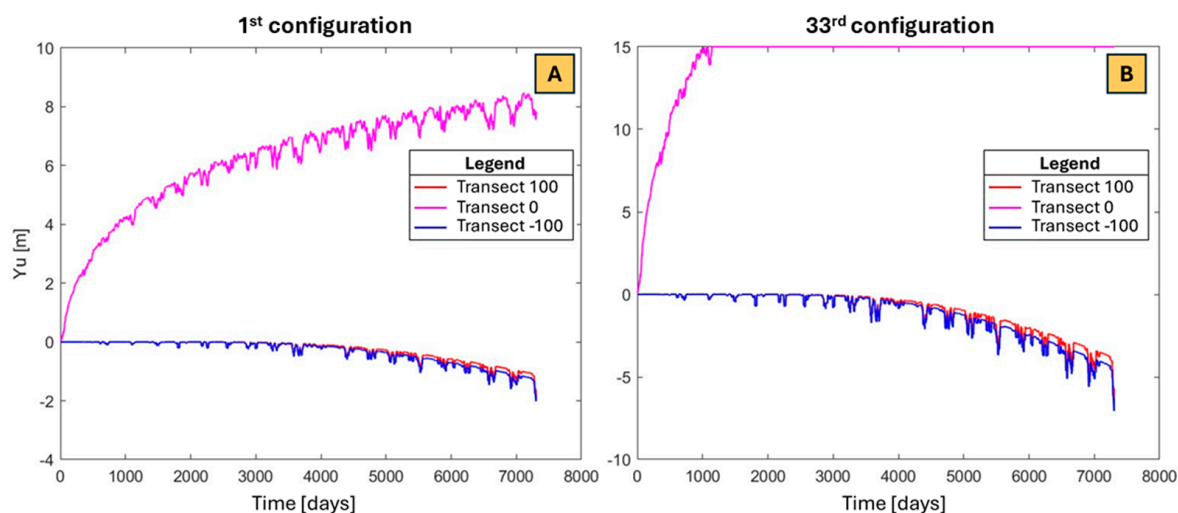


Figure 5. Development of Yu over time at the three selected transects, for the six selected configurations considering a 20-year simulation. Subplot (A) shows the trend for configuration 1 while the (B) for configuration 3.

In configuration 1 (subplot A), progressive and distributed sedimentation is observed along the transects closest to the breakwater middle section. The transect at 0 m shows a constant accumulation, with the shoreline position reaching and stabilising around 8 m after an initial period of rapid growth. The -100 transect shows a more moderate evolution, with its position stabilising just above zero, indicating that the breakwater, being at 175 m, does not generate a direct impact on this section. On the contrary, the transect at 100 m shows a progressive retreat of the shoreline, which stabilises around -2 m, signalling constant erosion in that area. This behaviour suggests that the rearmost position of the breakwater allows a more distributed accumulation of sediment along the shoreline but does not eliminate erosion phenomena in areas further from its direct field of influence.

In configuration 33 (subplot B), the effect of the reduced distance between the breakwater and the shoreline is immediately evident. The 0 transect shows much more intense accumulation than in configuration 1, with the shoreline stabilising at around 15 m, showing a more pronounced sediment trapping effect, indicating the formation of a tombolo. This phenomenon reflects highly localised sedimentation that interrupts sediment transport along the coast. At the same time, the transect at -100 and 100 m undergoes significant erosion, with the shoreline receding to lower values than in configuration 1, highlighting how the localised influence of the breakwater accentuates sediment removal in the lateral areas.

The comparison between the two configurations clearly highlights the importance of the position of the breakwater in modulating sediment transport and accumulation processes. In configuration 1, the greater distance of the breakwater from the coast allows for more gradual and diffuse sedimentation, limiting extreme phenomena such as the formation of tombolo, but does not completely eliminate erosion in the more distant transects. On the contrary, in configuration 33, the proximity of the breakwater generates an intense and localised accumulation of sediment, culminating in the formation of a tombolo, to the detriment, however, of the nearby areas, which undergo more accentuated erosion. This analysis underlines how the design of coastal defence works must carefully consider not only local protection objectives but also the long-term impacts on the sediment balance and morphodynamic equilibrium of adjacent areas.

3.2. Groyne Analytical Validation Results

After carrying out a one-year simulation, Figure 6 shows the comparison of the results obtained with COAST-PRO_{SIM}, shown as a red dashed line in the graph below, with those

obtained through the method proposed by Valsamidis and Reeve, used in this work as a reference method, shown as blue dots.

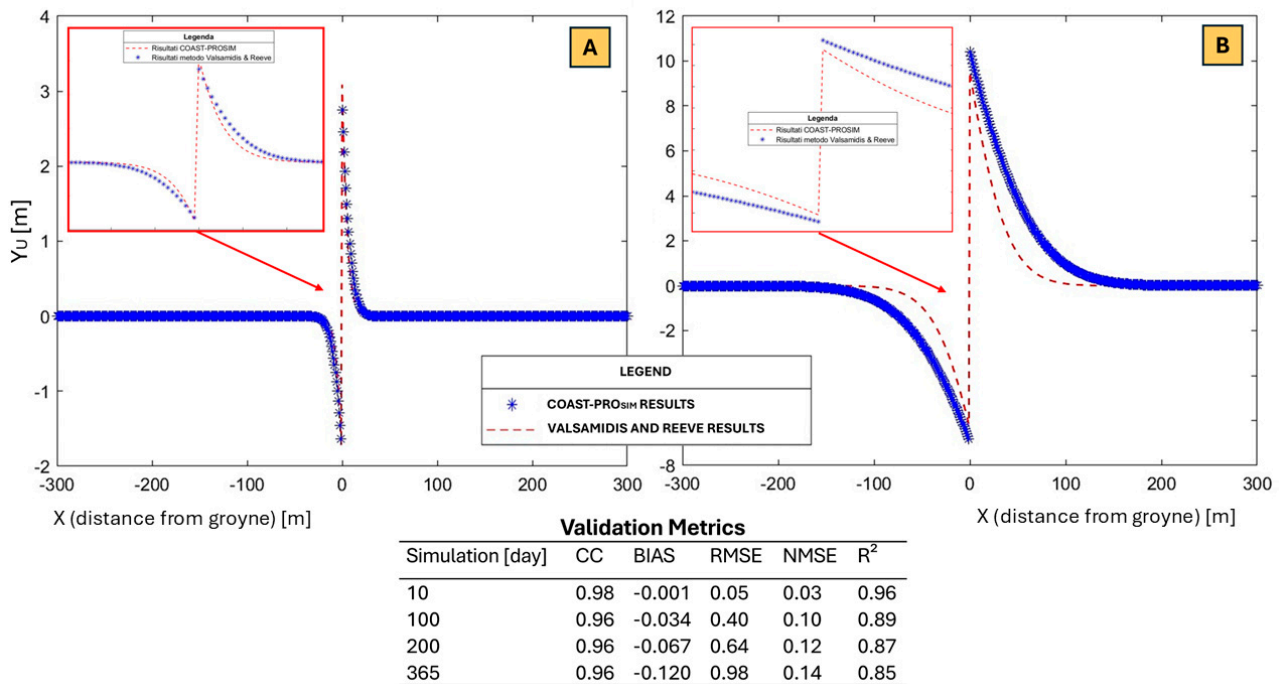


Figure 6. Comparison of results obtained with COAST-PRO_{SIM} and the method proposed by A. Valsamidis and D. E. Reeve on different simulation days (subplot (A) and (B) respectively for 10 and 365 days) considering a total simulation duration of 1 year.

The first analysis shows a remarkable concordance between the values obtained by the two methods, particularly in the first 10 days of simulation, then deviating slightly as time progresses (subplot A of Figure 6).

For an analytical comparison, see the table reported at the bottom of Figure 6; the relative values of the chosen validation metrics were calculated for several arbitrarily chosen time instants and considered representative, in particular, after 10, 100, 200, and 365 days.

From the comparative analysis, the values obtained indicate that COAST-PRO_{SIM} is adequate for the prediction of the shoreline following the insertion of a semi-permeable groyne. Although the results vary negligibly as the number of simulation days increases, they remain consistent.

The correlation coefficient approaches a value of 1 already after a few days of simulation, deviating by only about 2% after one year. The BIAS remains negative, showing no significant over- or underestimates. The RMSE value remains low, suggesting good accuracy. The NMSE value is very close to 0, while the coefficient of determination R² is at a rather high level.

The shoreline location simulation, obtained by solving Equation (2), was further conducted over a period of 20 years, with daily simulations. For illustrative purposes, Figure 7 presents the solution for 12 arbitrarily chosen simulation days. In particular, day 1, day 100, day 200, and day 365, corresponding to one year from the simulation; day 500, representing the middle of the second year, useful for observing changes after another annual cycle; day 1000, to analyse how the dynamics change on a multi-year scale; day 1500, about four and a half years, representing an intermediate point in the long-term simulation; day 2000 and day 3000, about eight and a half years, showing longer-term changes; day

5000, after some thirteen and a half years of simulation; and finally, day 7305, representing the final situation after twenty years of simulation.

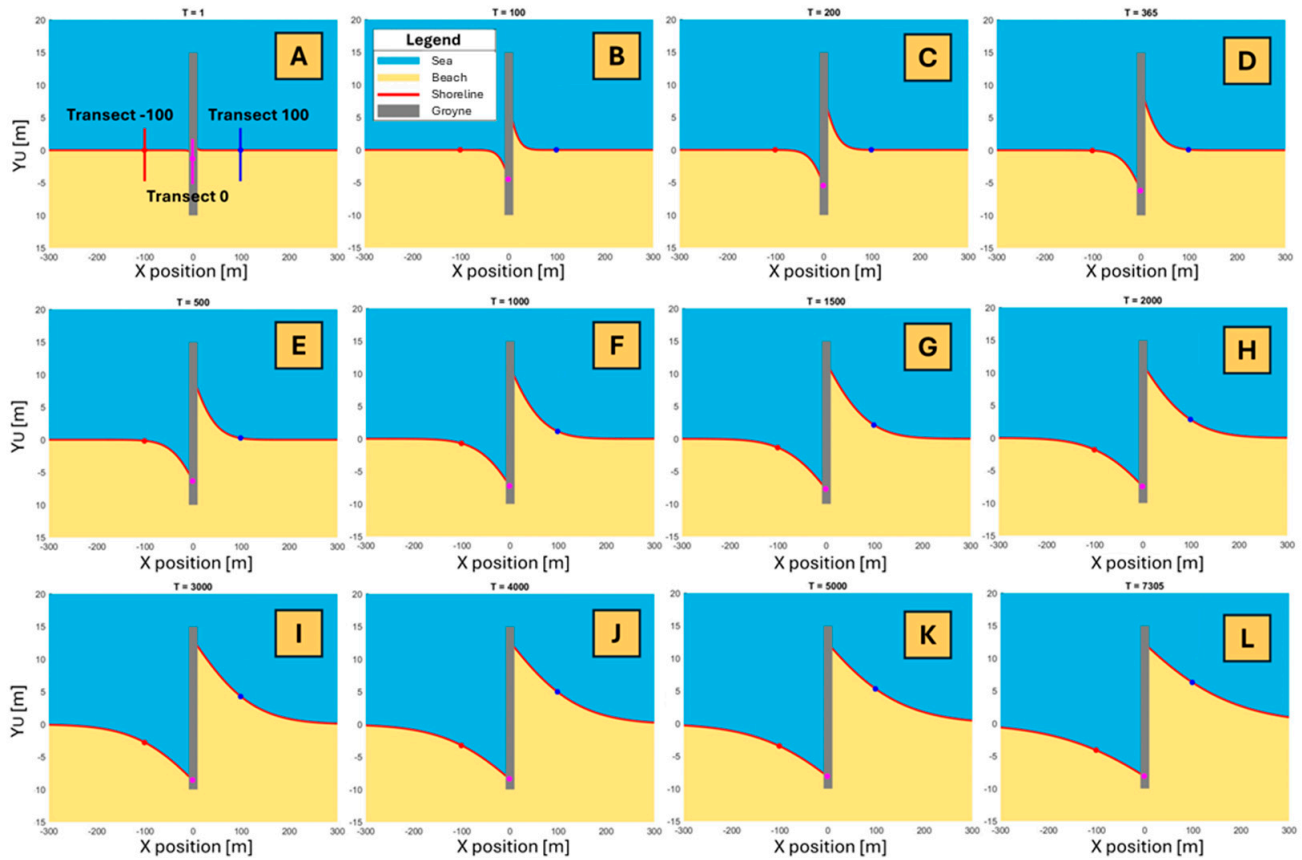


Figure 7. Trend of Y_u for 12 selected simulation days (from A–L) considering an overall simulation of 20 years. Indication of time is provided as the title of each subplot.

Figure 7 shows, highlighted as a red line, the evolution of the shoreline as the number of simulation days increases; in grey is the groyne, which, as shown in Table 1 has a length of 15 m. Note that the following three transects are highlighted in the graph for simulation day 1: Transect -100 in red; Transect 0 in magenta; and Transect 100 in blue. This colour coding is also kept constant in the graphs of subsequent configurations. The results of the numerical simulation show a significant shoreline evolution in response to the presence of the groyne. In the first 100 days, a shoreline retreat of about 5 m is observed to the left of the groyne (in the upwave zone) due to the interruption of sediment transport along the coast. At the same time, there is an advancement of an equal magnitude to the right of the breakwater (in the under-billow zone) due to the accumulation of sediment diverted by the breakwater, which allows a partial passage of sediment but limits erosion in the area above the breakwater. At full regime, after 20 years, the advancement of the shoreline reaches a maximum of 12 m, while the retreat is about -9 m. This difference between advancement and retreat results from the semi-permeable nature of the groyne. The analysis of erosion and accretion rates indicates that the most significant variations occur during the first year of the simulation, with a progressive decrease over time.

Figure 8 confirms this trend, showing how the changes in the position of the shoreline are more pronounced in the early days of the simulation. This figure shows the trend of the shoreline Y_u as time changes for seven selected simulation days (subplot A), from day 1 to day 7305 (same as previous).

Figure 8 represents the results of the movement of the shoreline and transects over time at a fixed breakwater. Subplot A illustrates the evolution of the position of the shoreline

(Y_u) along a horizontal x axis, representing the distance to the breakwater (located at $x = 0$), at different temporal moments. Subplot B, on the other hand, shows the variation in Y_u over time for three distinct transects (-100 m, 0 m, and 100 m).

In subplot A, it is evident how the breakwater generates significant sediment accumulation on the upwave side ($x > 0$) and marked erosion downwave ($x < 0$). In the first few days (day 10 and day 200), a gradual advance of the upwave shoreline is observed, accompanied by a gradual retreat of the downwave shoreline. As time increases (up to day 7300), accumulation on the windward side reaches a stable plateau, with values exceeding 15 m, while on the leeward side, erosion intensifies until it stabilises at values close to -8 m. These results highlight the direct impact of the breakwater on retaining sediment moving along the shoreline, significantly altering the profile of the shoreline in both positive and negative directions with respect to the structure.

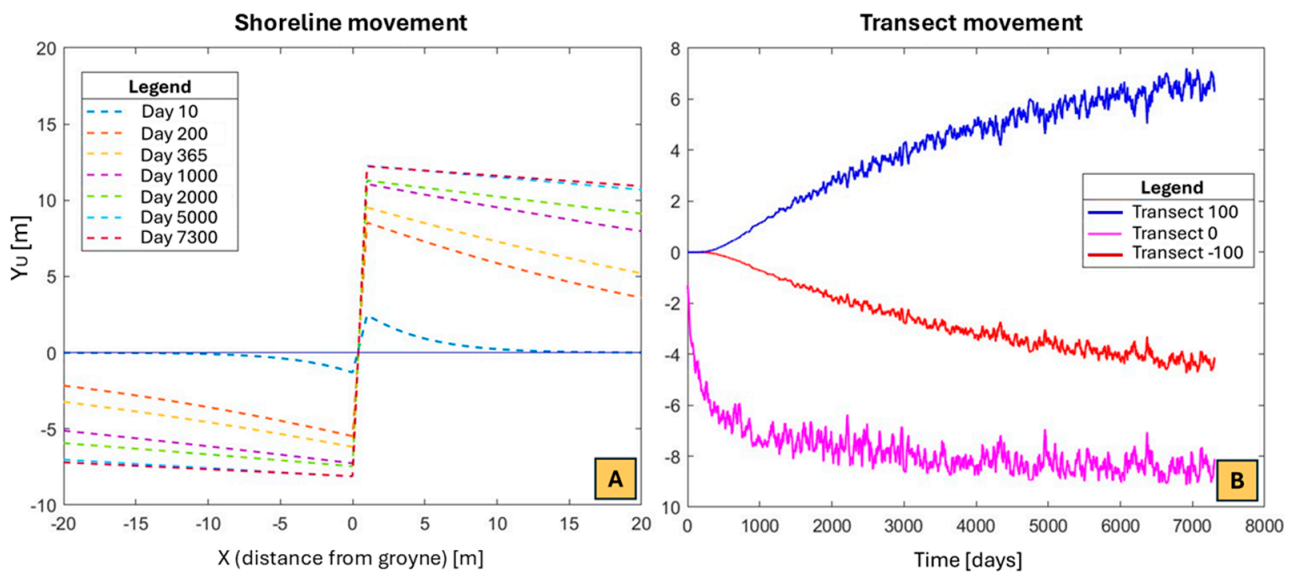


Figure 8. Development of Y_u as time changes for seven selected simulation days, considering a total simulation period of 20 years. Subplot (A) depicts the shoreline movement for all transects between -20 and $+20$ m. Subplot (B) shows the shoreline trend for transects -100 , 0 and 100 through time.

Subplot B analyses in detail the temporal evolution of the shoreline in the three specific transects. The central 0 m transect (magenta curve), the transect immediately downwave, shows progressive erosion, with Y_u decreasing rapidly in the first few years and then stabilising around -8 m. The -100 transect (red curve) initially fluctuates around 0 m but stabilises towards the -3.5 m value indicating further erosion in the downwave zone even at a 100 m distance. The 100 m transect (blue curve) shows marked sediment accumulation, with Y_u steadily increasing to over 6 m. This behaviour reflects the trapping of sediment by the breakwater on the upwave side, while the lack of sediment transport downwave generates progressive erosion.

In addition, all three curves show oscillations around the general trend. These oscillations are due to the interaction between wave motion and sedimentary dynamics, which COAST-PRO_{SIM} takes into account. The oscillations become more pronounced as time passes. This could be because, initially, the system is dominated by processes of adaptation to the new condition imposed by the groyne, while later, more complex mechanisms related to the interaction between wave motion and bottom morphology come into play. These observations are in line with the idea that cross-shore transport plays an important role in sedimentary dynamics. Wave motion suspends sediments, which are then transported along the profile under the action of wave-induced currents. This process generates

fluctuations in the amount of sediment present at a given point, which are reflected in the fluctuations of the parameter considered.

3.3. Study Area Application Results

3.3.1. San Leone Application Results

In this work, COAST-PRO_{SIM} was applied for the prediction of the shoreline following the construction of six breakwaters, shown in Figure 9, and its results were subsequently compared with shoreline observations detected from satellite images. Subplot A represents the real planimetric position using the WGS84 UTM 33N reference system. In the same subplot, the shoreline “baseline” is indicated, which serves as an initial reference for time comparisons. In subplot B, the planimetric view was rotated in order to make the shoreline sub-horizontal. Subplot C shows the location of the beach studied in relation to the entire Sicilian Island.

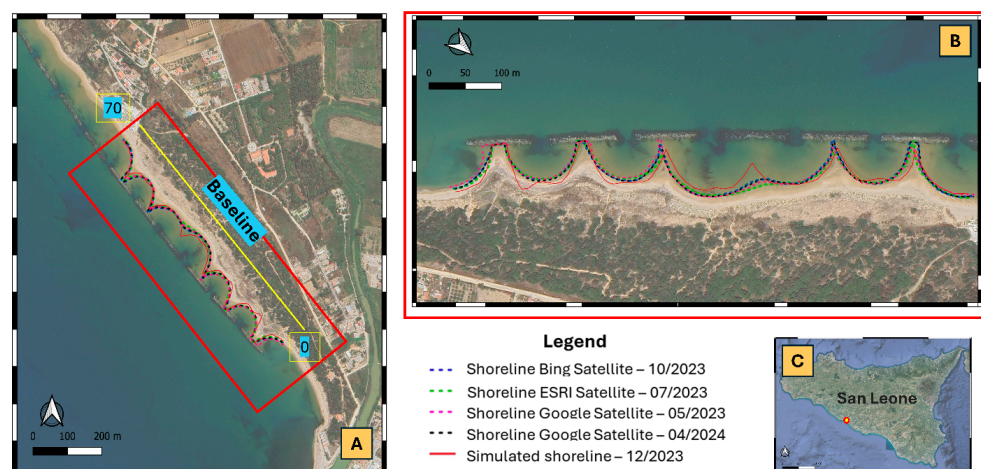


Figure 9. San Leone study area. Subplot (A) shows the planimetric position of the study area while subplot (B) the horizontal view. In subplot (C) the position of the area in Sicily is provided. SR: WGS84 UTM 33N–32633.

Considering a horizontal shoreline development, in Figure 9, the shoreline simulated by the model and the four shorelines detected from satellite images are shown on the left, and the deviation between the model results and the comparison observations is shown on the right. From a first visual analysis, it is possible to see an overestimation of advancement at breakwater No. 4 (starting from the left in subplot B of Figure 9) where the observations report a lesser advancement, probably due to the fact that the drift in the opposite direction was interrupted due to the deposition caused by the presence of the structures.

From the analysis of the deviations (right panel in Figure 10), however, the greatest difference between the model and observations is evident at barrier No. 6, where the model does not predict the formation of a tombolo on the last day of the simulation (December 2023), which is instead found in the observations of the satellite images. Quantitatively, the deviations between the simulated and observed shorelines reach the maximum negative value of -47 m compared to the Google Satellite images on May 2023 and the maximum positive difference of $+31$ m compared to the ESRI Satellite images on July 2023 precisely at barrier No. 3.

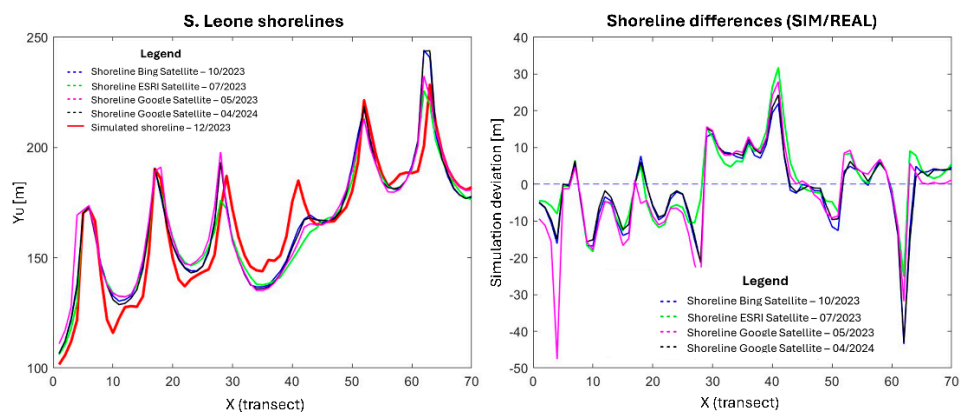


Figure 10. (Left): the shoreline simulated by the model and the four shorelines observed from satellite images; (Right): the deviation between the model results and the San Leone comparison observations.

The comparative analysis between the model results and satellite observations shows a high accuracy in predicting the coastline. With a tolerance of 10, 15, and 20 m, the model has an accurate prediction rate of 68% to 77%, 85% to 90%, and 92% to 96%, respectively (Table 4). These results indicate that the model is able to capture the coastal dynamics of the studied sites with good approximation.

Table 4. Percentage of accurate predictions of COAST-PRO_{SIM} for different tolerances and satellite image acquisition periods for San Leone beach.

Tolerance (m)	Bing (October 2023)	ESRI (July 2023)	Google (May 2023)	Google (March 2024)
10	73%	77%	68%	76%
15	89%	90%	85%	89%
20	96%	96%	95%	92%

Table 5 shows the values of the chosen validation metrics for the comparison between simulated data from COAST-PRO_{SIM} and observations from satellite imagery.

Table 5. Analytical comparison between the results obtained with the COAST-PRO_{SIM} model and observations from satellite images with relative values of the chosen validation metrics, correlation coefficient, BIAS, RMSE, NMSE, and coefficient of determination R², for San Leone beach.

	Validation Metrics Between Simulated and Observed Data			
	Bing (October 2023)	ESRI (July 2023)	Google (May 2023)	Google (March 2024)
CC	0.93	0.94	0.90	0.93
BIAS	−1.39	0.17	−2.01	−0.84
RMSE	10.35	9.63	12.25	10.23
NMSE	0.14	0.14	0.23	0.13
R ²	0.85	0.85	0.77	0.86

Analytical comparison of the values obtained indicated that COAST-PRO_{SIM} is suitable for predicting the shoreline of San Leone beach following the insertion of the six breakwaters.

The statistical analysis showed a high correlation between the model results and the observed data, with a correlation coefficient close to 1. The BIAS, slightly negative for the Bing Satellite (October 2023) and Google Satellite (May 2023 and March 2024) images, indicates a slight tendency for the model to underestimate erosion. The RMSE and NMSE confirm the good accuracy of the predictions, and the coefficient of determination R² is quite high.

The results show the model's ability to reproduce the formation of tombolos at the first barrier, after approximately day 3000 of simulation, and at the second barrier at the end of the simulation, as well as the formation of salients for the others. Furthermore, the model reproduces the oscillations of the coastline due to the interaction with wave motion. In particular, it can be observed that the oscillations are less pronounced in the early stages of the simulation and become more pronounced later on due to the greater amount of sediment in suspension. An example of this behaviour is presented in Figure 11 (bottom subplot).

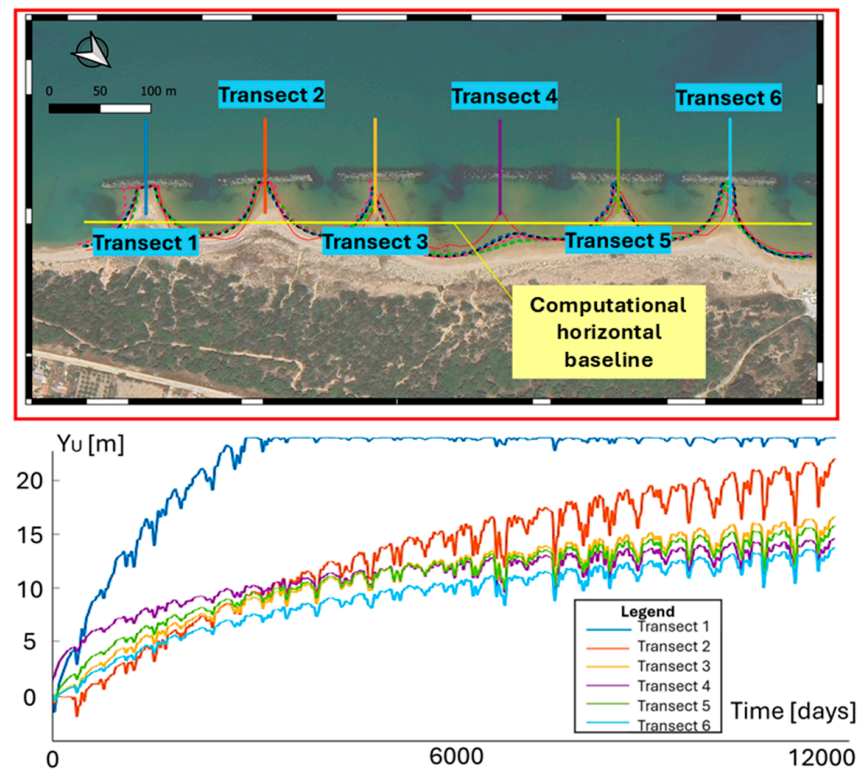


Figure 11. On the left is the shoreline simulated with COAST-PRO_{SIM} for San Leone beach in its final configuration in December 2023, and on the right is the trend at the transects. Dashed lines in the upper subplot represent the shoreline position presented in Figure 9. Colours of different transects (upper panel) are respected in the bottom panel.

3.3.2. Porto Empedocle Application Results

As already anticipated, COAST-PRO_{SIM} was applied for the prediction of the shoreline following the construction of the harbour, the inner arm of which is treated as a long impermeable groyne, shown in Figure 12, and its results were subsequently compared with shoreline observations from satellite images.

Subplot A (Figure 12) represents the actual planimetric position in SR WGS84 UTM 33 N. Subplot B shows the schematisation of the model. Subplot C shows the development of the satellite and simulated coastlines at the end of the simulation, while subplot D shows the location of the area under examination on the southern Sicilian coast.

It should be noted that only the under-billow zone of the harbour, characterised by sediment accumulation, has been dealt with. The area above the groyne, which is characterised by erosion, is omitted, making the erosion phenomenon irrelevant for this specific area.

The same procedure as that described in the case study for San Leone beach was used to characterise the meteomarine climate.

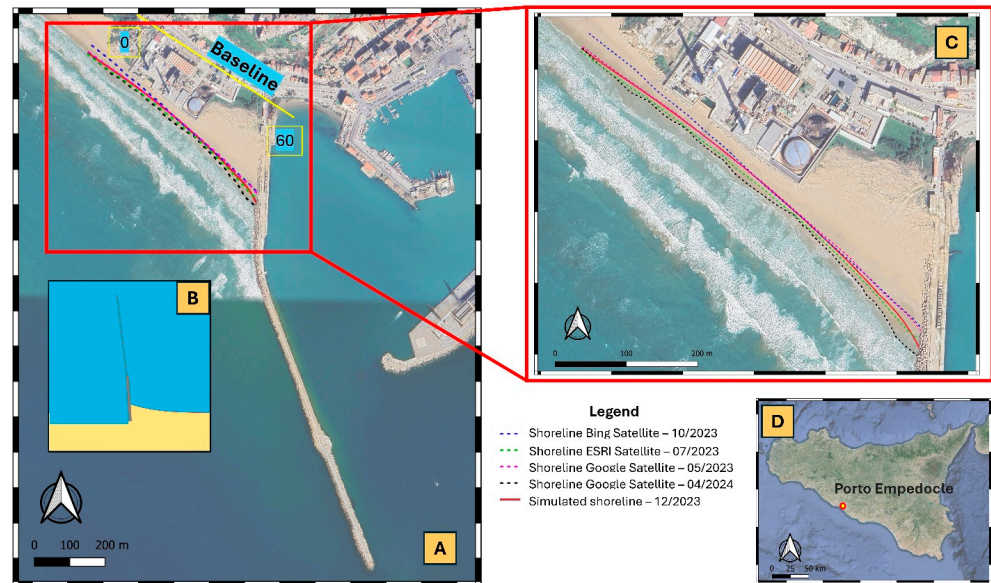


Figure 12. Porto Empedocle study area with shorelines. Subplot (A) shows the planimetric position of the study area while subplot (C) a zoomed-in view. Subplot (B) is the model result depicting harbour arm, beach and sea. In subplot (D) the position of the area in Sicily is provided.

Considering horizontal shoreline development, in Figure 13, the shoreline simulated by the model and the four shorelines observed from satellite images are shown on the left, and the deviation between the model results and the comparison observations is shown on the right. From a first visual analysis, it is possible to see how the five shorelines do not overlap, with differences between the various observations as well.

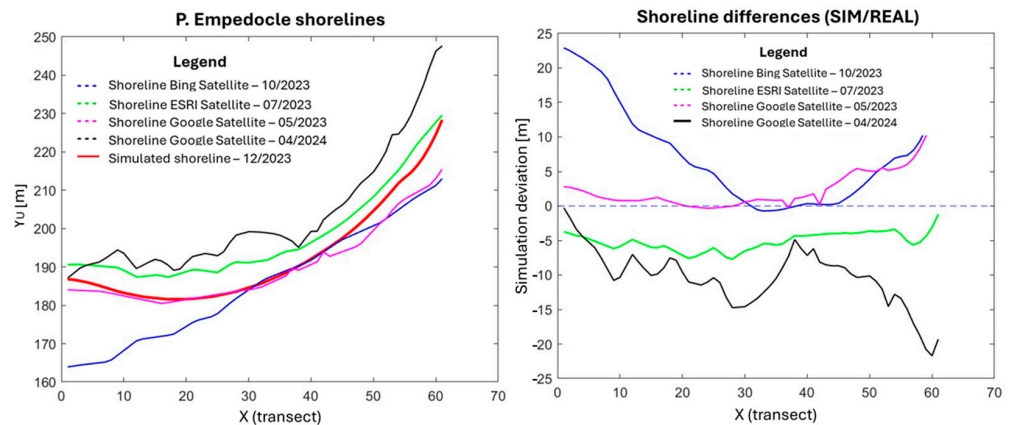


Figure 13. (Left): the shoreline simulated by the model and the four shorelines observed from satellite images; (Right): the deviation between the model results and the comparison observations.

From the analysis of the deviations (right panel of Figure 13), on the other hand, the greatest difference between the model and observations is evident in the area immediately behind the harbour arm. Quantitatively, the deviations between the simulated and observed shorelines reach the maximum negative value of -21 m compared to the Google Satellite images in March 2024 and the maximum positive difference of $+22$ m compared to the Bing Satellite images in October 2023.

The comparative analysis of the results for Porto Empedocle showed greater accuracy in the model's ability to predict the coastline than for San Leone (Figure 10). In particular, with tolerances of 20 m, there is always an accuracy above 90%, and for a tolerance of 10 m, the accuracy is never less than 70% (Table 6).

Table 6. Percentage of accurate predictions of COAST-PRO_{SIM} for different tolerances and satellite image acquisition periods for Porto Empedocle beach.

Tolerance [m]	Bing (October 2023)	ESRI (July 2023)	Google (May 2023)	Google (March 2024)
10	70%	100%	50%	96%
15	82%	100%	92%	100%
20	90%	100%	97%	100%

In Table 7, the values of the chosen validation metrics for the comparison between simulated data from the COAST-PRO_{SIM} model and observations from satellite imagery are shown.

Table 7. Analytical comparison between the results obtained with the COAST-PRO_{SIM} model and observations from satellite images with relative values of the validation metrics, correlation coefficient, BIAS, RMSE, NMSE, and coefficient of determination R^2 , for Porto Empedocle beach.

Validation Metrics Between Simulated and Observed Data				
	Bing (October 2023)	ESRI (July 2023)	Google (May 2023)	Google (March 2024)
CC	0.88	0.99	0.99	0.98
BIAS	7.24	−5.13	2.47	−10.35
RMSE	10.09	5.30	3.84	11.14
NMSE	0.46	0.20	0.15	0.51
R^2	0.53	0.80	0.85	0.48

Analytical comparison of the values obtained indicated that COAST-PRO_{SIM} is suitable for the prediction of the shoreline of Porto Empedocle beach following the insertion of a groyne.

The correlation coefficient is very close to a value of 1, the lowest value being for the Bing Satellite observation dated October 2023. The BIAS has slightly different values; it is positive when compared with the Bing Satellite images from October 2023 and the Google Satellite images from May 2023, indicating an, albeit negligible, overestimation of the model. In contrast, it remains negative for ESRI Satellite's July 2023 and Google Satellite's March 2024 images. The RMSE value remains within the same order of magnitude for all four comparison images, indicating no substantial differences. The value of NMSE is close to 0, and finally, the coefficient of determination R^2 is quite high when compared with the 2023 images for the ESRI Satellite and Google Satellite.

Again, the results of the simulation reveal the model's ability to reproduce the position of the shoreline at a groyne, and the graph on the right shows that the model reproduces the oscillations of the shoreline due to the interaction with wave motion. As in the previous case concerning San Leone beach, the oscillations are less pronounced in the early stages of the simulation, becoming more pronounced later.

3.3.3. Villafranca Tirrena Application Results

The COAST-PRO_{SIM} model was applied for the prediction of the shoreline following the construction of five groynes, shown in Figure 14, and its results were subsequently compared with observations from satellite images.

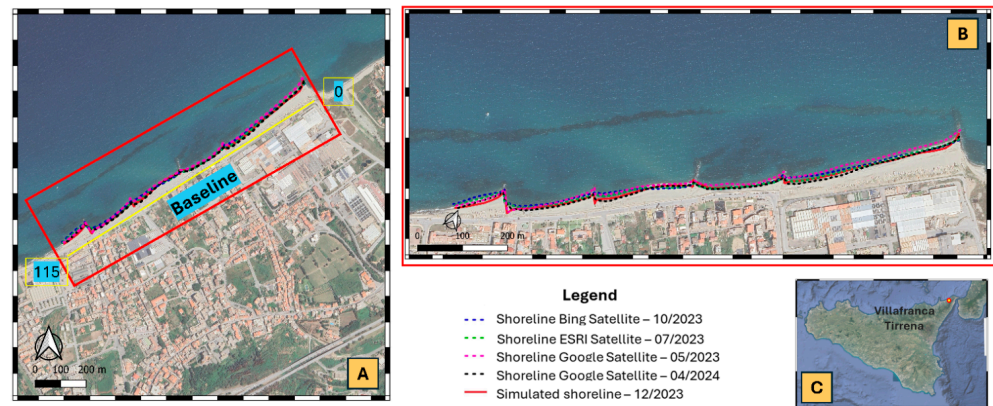


Figure 14. Villafranca Tirrena study area. Same SR as previous figures. Description of subplots is the same reported in Figure 9.

Subplot A represents a satellite image that includes the entire study area, delimited in red. The “baseline” shoreline is indicated, which serves as an initial reference for temporal comparisons. The area is characterised by the presence of groynes orthogonal to the coastline. Subplot B provides shoreline detail along the segments protected by the groynes. The different shorelines are also shown, corresponding to the satellite observations and the numerical simulation predicted for December 2023. The observed (blue, green, and purple) and simulated (red) shorelines show good agreement between the numerical and satellite data. Finally, subplot C shows the geographical position of the study area in the regional context, locating it along the northeast coast of Sicily.

Considering a horizontal shoreline development, Figure 15 (left panel) shows the shoreline simulated by the model and the four shorelines observed from satellite images, and the deviation between the model results and the comparison observations is shown below. From a first visual analysis, it is possible to see the absence of any particular areas of overestimation or underestimation of the model compared to the observations.

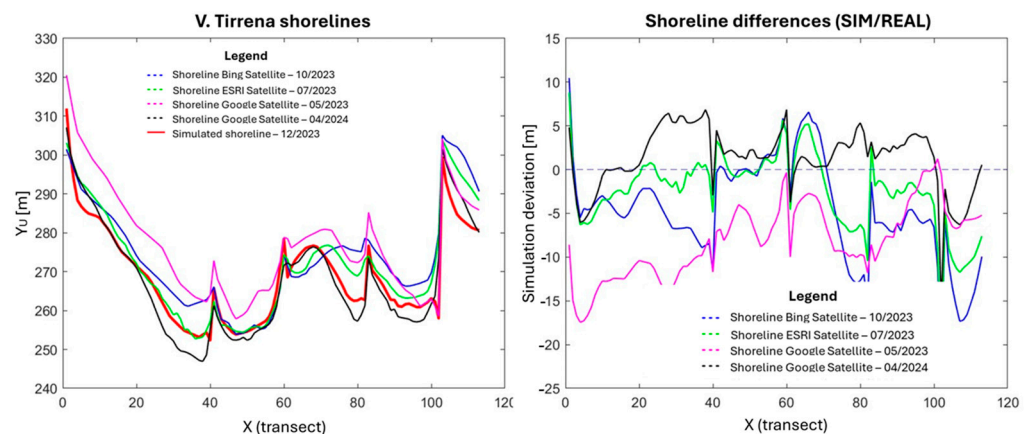


Figure 15. (Left): the shoreline simulated by the model and the four shorelines observed from satellite images; (Right): the deviation between the model results and the Villafranca Tirrena comparison observations.

On the other hand, the analysis of the deviations (right panel of Figure 15) shows a negative deviation from the observations of the Google Satellite images dated May 2023 and a positive deviation from the Google Satellite images dated March 2024. Quantitatively, the deviations between the simulated and observed shorelines reach the maximum negative value of -21 m compared to the Bing Satellite images dated October 2023 and the maximum positive difference of $+10$ m compared to the same satellite images.

Analysing the comparison with satellite image observations, it appears that the model is able to accurately predict the position of the shoreline. Specifically, with a tolerance of 10 m, the results on the deviation between the simulated and actual shorelines are as follows.

The comparative analysis of the results for Villafranca Tirrena showed excellent accuracy in the model's ability to predict the coastline. In particular, with tolerances of 20 m, there is always an accuracy of over 99%, and for a tolerance of 10 m, while reaching an accuracy of less than 70% for the year 2024, this exceeds 80% for the observations of the year 2023 (Table 8).

Table 8. Percentage of accurate predictions of COAST-PRO_{SIM} for different tolerances and satellite image acquisition periods for Villafranca Tirrena beach.

Tolerance (m)	Bing (October 2023)	ESRI (July 2023)	Google (May 2023)	Google (March 2024)
10	83%	93%	99%	67%
15	94%	99%	99%	96%
20	99%	99%	100%	100%

Table 9 shows the values of the chosen validation metrics for the comparison between simulated data from the COAST-PRO_{SIM} model and observations from satellite imagery.

Table 9. Analytical comparison between the results obtained with the COAST-PRO_{SIM} model and observations from satellite images with relative values of the validation metrics, correlation coefficient, BIAS, RMSE, NMSE, and coefficient of determination R^2 , for Villafranca Tirrena beach.

	Validation Metrics Between Simulated and Observed Data			
	Bing (October 2023)	ESRI (July 2023)	Google (May 2023)	Google (March 2024)
CC	0.90	0.95	0.95	0.98
BIAS	−4.64	−2.46	−8.12	1.30
RMSE	7.41	4.99	9.12	3.81
NMSE	0.31	0.13	0.45	0.07
R^2	0.68	0.86	0.54	0.93

Analytical comparison of the values obtained indicated that COAST-PRO_{SIM} is suitable for predicting the shoreline of the beach of Villafranca Tirrena following the construction of five groynes.

The correlation coefficient is very close to a value of 1, reaching maximum values when compared to the Google Satellite images of March 2024. The BIAS is negative when compared with Bing Satellite images from October 2023, ESRI Satellite images from July 2023, and Google Satellite images from May 2023, indicating a slight underestimation of the model. However, the BIAS is positive for the Google Satellite images of March 2024. The RMSE value is similar for all four comparison images, suggesting no substantial differences between them. The value of NMSE is close to 0, with better performance for the Google Satellite images of March 2024. Finally, the coefficient of determination R^2 is relatively high, with optimal results again for the March 2024 Google Satellite images. These results indicate that the Google Satellite images are the most accurate in representing the simulated shoreline.

3.4. Computation Time

All simulations were run on a powerful desktop computer equipped with a Windows 10 operating system, a 3.00 GHz Intel Core i9-13900K processor, and 32 GB RAM.

The case study of Porto Empedocle, characterised by a relatively simple geometry and a limited study area, took approximately five minutes to calculate. The case studies of San

Leone and Villafranca Tirrena, with more complex geometries and larger study areas, took approximately 30 min and 20 min of calculation time, respectively.

These results highlight one of the main strengths of the model: its ability to provide accurate results with extremely fast calculation times, making it an ideal tool for scenario analysis and decision making in coastal engineering.

4. Conclusions

This paper proposes an innovative simulation model for evaluating the effectiveness of coastal protection structures. It stands out for its ability to integrate a variety of variables and phenomena that influence shoreline evolution, making it a versatile tool for analysing coastal dynamics.

The simulations carried out on real case studies, including San Leone, Porto Empedocle, and Villafranca Tirrena, highlighted the model's ability to provide detailed and reliable predictions of the evolution of the coastline in the presence of protection structures day by day. The model achieved high accuracy (10–12 m maximum error over about 30 years) while reducing computational times compared to traditional models. For instance, traditional one-line models, commonly used for shoreline evolution studies, require hours for simulations across the same time span, with errors ranging from 20 to 90 m, depending on the wave climate and model assumptions (as seen in Baptista et al. [85] and Pombo et al. [26]). The results obtained show that the model can be used effectively as a support tool for coastal planning, adapting to the geographical and environmental specificities of different contexts. This flexibility makes its application to a wider range of coastal environments possible, making a significant contribution to the sustainable management of coastal resources.

The presented COAST-PROSIM model is not without limitations. Firstly, the model assumes that sediment transport is limited to the region extending to the closure depth, which may oversimplify sediment dynamics in areas with significant offshore transport or highly complex bathymetric features. Additionally, the model's reliance on simplified assumptions for wave propagation and sediment transport might lead to inaccuracies in environments where three-dimensional processes, such as rip currents or complex wave refraction, dominate.

COAST-PRO_{SIM} fills some of the gaps in traditional models in terms of efficiency, adaptability, and computational effort, as demonstrated in the validation tests and case study applications presented. Although the use of COAST-PRO_{SIM} and similar models requires the availability of high-quality data and access to adequate computational resources, it appears that they are an indispensable tool for understanding the complex dynamics of erosion and sedimentation, as well as for assessing the impact of natural phenomena and anthropogenic interventions. Indeed, the ability to simulate future scenarios related to climate change, extreme events, and variations in sediment transport makes it possible to anticipate the potential consequences of human actions and natural phenomena. This is particularly important in the context of the increasing vulnerability of coastal areas, where threats associated with climate change, such as sea-level rise and the increased frequency of extreme weather and sea events, make the adoption of adaptation and mitigation strategies urgent. For example, using forcings input data that consider more extreme meteorological and marine climate scenarios allows, from a management and analysis perspective, for the simulation of the behaviour of structures in coastal dynamics, allowing timely action.

Future developments of the model aim to enhance its capabilities by incorporating the simulation of both protected and unprotected beach nourishment interventions, as well as expanding its scope to include the effects of seawalls on coastal dynamics.

Author Contributions: Conceptualisation, P.S., G.M. and G.C.; methodology, P.S. and G.C.; software, P.S.; validation, P.S. and L.C.C.; formal analysis, P.S. and L.C.C.; investigation, P.S.; resources, G.C.; data curation, P.S. and L.C.C.; writing—original draft preparation, P.S. and L.C.C.; writing—review and editing, P.S., G.M. and G.C.; visualisation, P.S. and L.C.C.; supervision, G.C. and G.M. All authors have read and agreed to the published version of the manuscript.

Funding: This research received no external funding.

Data Availability Statement: The data presented in this study are available on request from the corresponding author.

Acknowledgments: This study was carried out within the RETURN Extended Partnership and received funding from the European Union Next-GenerationEU (National Recovery and Resilience Plan—NRRP—Mission 4, Component 2, Investment 1.3—D.D. 1243 2/8/2022, PE0000005).

Conflicts of Interest: The authors declare no conflicts of interest.

Appendix A

The analytical solution to Equation (12) in the main text is expressed as follows:

$$Y_{U1}(t) = Y A - Y e^{\frac{rad(a_b)}{Y} x + rad(a_b)^2 \times \frac{\varepsilon t 24}{Y^2}} B$$

Y is the length of the work considered (m).

The A term is defined as follows:

$$A = \operatorname{erfc}\left(\frac{x}{2\sqrt{\varepsilon t 24}}\right)$$

The B term is expressed by the following expression:

$$B = \operatorname{erfc}(rad(a_b)) \frac{\sqrt{(\varepsilon t 24)}}{Y} + \frac{x}{2\sqrt{\varepsilon t 24}}$$

The error function $\operatorname{erf}(z)$ is expressed as in the following:

$$\operatorname{erf}(z) = \frac{2}{\sqrt{\pi}} \int e^{-z^2} dz$$

Its complement $\operatorname{erfc}(z)$ is given by the following equation:

$$\operatorname{erfc}(z) = 1 - \operatorname{erf}(z)$$

To determine when the structure reaches its maximum capacity, the time t_f (s) is calculated, which is the time at which the structure can no longer support further accumulation, equal to the following:

$$t_f = \frac{(Y^2 \pi)}{4 \varepsilon \tan^2 a_b}$$

Then, under the condition that $t > t_f$, the solution becomes as follows:

$$y = Y \operatorname{erfc}\left(\frac{x}{2\sqrt{\varepsilon t_2}}\right) \quad \text{per } t > t_f$$

This is valid with boundary conditions: $y = Y$ for $x = 0$ and $y = 0$ for $x = \infty$ for every $t > 0$.

Appendix B

In the following, the W term equation refers to Equation (14) in the main text.

$$W = \frac{H'_{s(b)}}{0.55 \times A}$$

where A represents the scale parameter of Dean's equilibrium profile, which depends on the sedimentation rate wf of the sediment and thus on characteristics such as size and density:

$$A = 0.5 \times wf^{0.44}$$

Dean developed a theory for the equilibrium profile of beaches, which describes how beaches are shaped in response to wave-induced sediment transport processes. His theory includes parameters such as sedimentation velocity and sediment size, which are crucial for predicting how sediment is distributed along the coast.

The depth at which the breaking occurs can be expressed by the following equation:

$$h_b = X_b s$$

in which s is the slope of the beach (equal to transects slope), and X_b is the distance of the breaker line from the surf-zone (m) and can be expressed as follows:

$$X_b = \frac{h_c}{s}$$

Appendix C

Appendix C.1. Correlation Coefficient, CC

The correlation coefficient (CC), or Pearson's coefficient, is expressed by the following equation and is used to quantify the strength of the linear relationship between the two predictions:

$$CC = \frac{\sum_{i=1}^n (\hat{y}_i - \bar{\hat{y}})(y_i - \bar{y})}{\sqrt{\sum_{i=1}^n (\hat{y}_i - \bar{\hat{y}})^2} \times \sqrt{\sum_{i=1}^n (y_i - \bar{y})^2}}$$

where n is the number of available values; \hat{y}_i are the values provided by COAST-PRO_{SIM}; y_i are the values predicted by the Silvester-Hsu method; $\bar{\hat{y}}$ is the mean of the values predicted by COAST-PRO_{SIM}; and \bar{y} is the average of the values predicted by the Silvester-Hsu method.

This coefficient takes values varying between -1 and 1 , and the result can be interpreted, respectively, as a perfect negative correlation, data perfectly aligned with a decreasing line (bisector of the second and fourth quadrants), and a perfect positive correlation, data perfectly aligned with an increasing line (bisector of the first and third quadrants).

In the case of a value equal to or close to 0 , the metric suggests no linear correlation, and the data are randomly distributed with no obvious linear pattern.

Appendix C.2. Mean Error, BIAS

BIAS (*mean error*) measures the tendency of the model to overestimate or underestimate the values predicted by the reference model. It measures the average difference between the values predicted by COAST-PRO_{SIM} and the values obtained by the Silvester-Hsu technique:

$$BIAS = \frac{1}{n} \sum_{i=1}^n (\hat{y}_i - y_i)$$

where n is the number of available values; \hat{y}_i are the values provided by COAST-PRO_{SIM}; and y_i are the values predicted by the Silvester–Hsu method.

The BIAS can take on any real value, positive or negative. The magnitude and sign provide information on the direction and magnitude of the model's systematic error. When the BIAS is zero, it means that, on average, the model does not show a tendency to overestimate or underestimate the comparison data, indicating a good balance in the predictions. Conversely, a positive BIAS suggests that the model tends to overestimate the comparison values—i.e., its predictions are generally higher than the observed data. If the BIAS is negative, it means that the model tends to underestimate the actual values, with predictions that are, on average, lower than what has been observed.

Appendix C.3. RMSE

The RMSE (*root mean square error*) provides a measure of the *root* mean square deviation between the values of the two models. It therefore provides a measure of the dispersion of the predictions from the observed values, penalising larger errors more heavily. The lower the RMSE, the better the performance of the model.

$$RMSE = \sqrt{\frac{1}{n} \sum_{i=1}^n (\hat{y}_i - y_i)^2}$$

where n is the number of available values; \hat{y}_i are the values provided by COAST-PRO_{SIM}; and y_i are the values predicted by the Silvester–Hsu method.

The RMSE can take values between 0 and ∞ . An RMSE value of zero indicates a perfect match between the model's predicted and observed values, suggesting that the predictions are accurate. When the RMSE is greater than zero, it means that errors exist between the predictions and the actual values. A higher RMSE indicates a larger average error in the forecasts. There is no theoretical upper limit for the RMSE, as it can increase indefinitely in the presence of very large errors.

Appendix C.4. Normalised Root Mean Square Error, NMSE

The NMSE is a normalised version of the MSE (*mean square error*), which facilitates comparisons between models on different scales. It is usually normalised with respect to the variance in the observed data.

$$NMSE = \frac{\sum_{i=1}^n (\hat{y}_i - y_i)^2}{\sum_{i=1}^n (\hat{y}_i - \bar{y})^2}$$

where n is the number of available values; \hat{y}_i are the values provided by COAST-PRO_{SIM}; y_i are the values predicted by the Silvester–Hsu method; and \bar{y} is the mean value of the values predicted by the Silvester–Hsu method.

The mean square error (MSE) can be expressed as follows:

$$MSE = \frac{1}{n} \sum_{i=1}^n (\hat{y}_i - y_i)^2$$

where n is the total number of observations; \hat{y}_i represents the model-predicted value from COAST-PRO_{SIM} for the i -th observation; and y_i represents the value predicted by the Silvester–Hsu method for the i -th observation.

Since the errors between the values predicted by the two models are squared, the MSE is sensitive to outliers, i.e., very large prediction errors, which can have a significant impact on the overall measurement. For this reason, the MSE is used in combination with other

metrics (such as RMSE, NMSE, and R^2) to provide a more comprehensive assessment of a model’s performance.

Variance is a statistical measure that quantifies the dispersion of data with respect to their mean. In other words, variance indicates how far the values of a set of data deviate, on average, from the arithmetic mean of that set. It is one of the most common measures of variability and is used to understand the distribution of data within a sample or population. For a population, variance is expressed by the following Equation.

$$\sigma^2 = \frac{1}{n} \sum_{i=1}^n (x_i - \mu)^2$$

where n is the total number of data points in the population; x_i is the value of the i th data point; and μ is the population mean.

An NMSE of zero indicates that the model perfectly predicts all values according to this reference method. When the NMSE is less than one, it means that the model is more accurate than using the average of the values predicted by the Silvester–Hsu method. An NMSE equal to one suggests that the accuracy of the model is equivalent to that obtained using the average of the values of the reference method. If the NMSE is greater than one, the model is less accurate than using the average of the values provided by the Silvester–Hsu method.

Appendix C.5. Coefficient of Determination R^2

The coefficient of determination R^2 represents the proportion of the variance in the data predicted by the reference method that is explained by the model. It is commonly used to assess the accuracy of a regression model, indicating how well the predicted data match with the reference data. It can be calculated using the following equation:

$$R^2 = 1 - \frac{\sum_{i=1}^n (\hat{y}_i - y_i)^2}{\sum_{i=1}^n (y_i - \bar{y})^2}$$

where n is the number of available values; \hat{y}_i are the i -th values provided by COAST-PRO_{SIM}; y_i are the i -th values predicted by the Silvester–Hsu method; and \bar{y} is the average of the values predicted by the Silvester–Hsu method.

An R^2 value of 1 indicates that the model perfectly explains the variance in the data, showing an ideal match between predictions and observations. Conversely, an R^2 of 0 means that the model cannot explain the variance in the data, being useless as a forecasting tool. When R^2 lies between 0 and 1, the model can only explain part of the variance in the data. Finally, a negative R^2 can occur if the predictive model is even worse than using the mean of the data from the Silvester–Hsu reference method.

Appendix D

In this appendix, the expressions of Equation (17) terms are presented (Section 2.4.3). Y_1^G is expressed as follows:

$$Y_1^G = \frac{1}{\pi} \left(\pi \int_0^t \varepsilon(u) du \right)^{-\frac{1}{2}} \int_0^{+\infty} g(\xi) \left[\exp \left(-\frac{(x - \xi)^2}{4 \int_0^t \varepsilon(u) du} \right) + \exp \left(-\frac{(x + \xi)^2}{4 \int_0^t \varepsilon(u) du} \right) \right] d\xi$$

Y_2^G is expressed as follows:

$$Y_2^G = \frac{2}{\pi} \int_0^{+\infty} \left(\int_0^t \exp \left(-\int_w^t [\omega^2 \varepsilon(u)] du \right) \tilde{q}(\omega, w) dw \right) \cos(\omega x) d\omega$$

Also, Y_3^G is expressed as follows:

$$Y_3^G = \frac{1}{\sqrt{\pi}} \int_0^t \varepsilon(w)j(w) \left(\frac{1}{\sqrt{\pi} \int_w^t \varepsilon(u)du} \exp\left(-\frac{x^2}{4 \int_w^t \varepsilon(u)du}\right) \right) dw$$

where $g(\xi)$ is the initial position of the coastline; ξ is a dummy variable used in the integration process; ω is the transformation variable used in the Fourier cosine transform operation; \tilde{q} is the Fourier cosine transformed variable of q , a parameter describing the flow of sediment from a sediment source or sink; w is a time-related variable; and finally, $j(w)$ is a groyne boundary condition.

On the other hand, as regards the semi-analytical solution for predicting shoreline evolution in the vicinity of a groyne compartment [68], a solution to the diffusive equation is used, derived via finite Fourier cosine transforms. This solution is given by the sum of the following four terms in the following equation:

$$y^{GC} = y_1^{GC} + y_2^{GC} + y_3^{GC} + y_4^{GC}$$

y^{GC} is the position of the coastline, while y_1^{GC} is expressed by the following Equation:

$$y_1^{GC} = \frac{1}{a} \bar{g}(0) + \frac{1}{a} \int_0^t \varepsilon(w)(j(w) - k(w) + \hat{s}(0, w))dw$$

y_2^{GC} is expressed as follows:

$$y_2^{GC} = \frac{2}{a} \sum_{\psi=1}^{+\infty} \cos\left(\frac{\psi\pi x}{a}\right) \hat{g}(\psi) \exp\left(-\int_0^t \frac{\pi^2 \psi^2}{a^2} \varepsilon(u)du\right)$$

y_3^{GC} is expressed by the following equation:

$$y_3^{GC} = \frac{2}{a} \sum_{\psi=1}^{+\infty} \cos\left(\frac{\psi\pi x}{a}\right) \int_0^t \exp\left(-\int_w^t \varepsilon(u) \left(\frac{\psi\pi}{a}\right)^2 du\right) (\varepsilon(u) \left((-1)^\psi j(w) - k(w)\right)) dw$$

y_4^{GC} is expressed below:

$$y_4^{GC} = \frac{2}{a} \sum_{\psi=1}^{+\infty} \cos\left(\frac{\psi\pi x}{a}\right) \int_0^t \exp\left(-\int_w^t \varepsilon(u) \left(\frac{\psi\pi}{a}\right)^2 du\right) \hat{s}(\psi, w) dw$$

In the equation, $g(x)$ represents the initial position of the coastline expressed as follows:

$$\hat{g}(\psi) = \int_0^a g(x) \cos\left(\frac{\psi\pi x}{a}\right) dx \text{ per cui } \hat{g}(0) = \int_0^a g(x) dx$$

a is the length of the barrier compartment; $\hat{g}(\psi)$ is the finite cosine Fourier transform of $g(x)$; ψ is an integer transformation variable; $j(w)$ is the time-varying boundary condition on the left side of the groyne compartment; $k(w)$ is the boundary condition corresponding to the right-hand side of the groyne compartment; w is a dummy variable of integration; and \hat{s} is the source term given by the expression in the following Equation:

$$\hat{s}(0, w) = \int_0^a s(x, w) dx$$

References

- Luijendijk, A.; Hagenaars, G.; Ranasinghe, R.; Baart, F.; Donchyts, G.; Aarninkhof, S. The State of the World's Beaches. *Sci. Rep.* **2018**, *8*, 6641. [CrossRef] [PubMed]
- Mejjad, N.; Rossi, A.; Pavel, A.B. The Coastal Tourism Industry in the Mediterranean: A Critical Review of the Socio-Economic and Environmental Pressures & Impacts. *Tour. Manag. Perspect.* **2022**, *44*, 101007. [CrossRef]
- Scala, P.; Toimil, A.; Álvarez-Cuesta, M.; Manno, G.; Ciraolo, G. Mapping Decadal Land Cover Dynamics in Sicily's Coastal Regions. *Sci. Rep.* **2024**, *14*, 22222. [CrossRef] [PubMed]
- Crain, C.M.; Halpern, B.S.; Beck, M.W.; Kappel, C.V. Understanding and Managing Human Threats to the Coastal Marine Environment. *Ann. N. Y. Acad. Sci.* **2009**, *1162*, 39–62. [CrossRef]
- de Gracia, A.; Rangel-Buitrago, N.; Oakley, J.A.; Williams, A. Use of Ecosystems in Coastal Erosion Management. *Ocean Coast. Manag.* **2018**, *156*, 277–289. [CrossRef]
- Sahavacharin, A.; Sompongchaiyakul, P.; Thaitakoo, D. The Effects of Land-Based Change on Coastal Ecosystems. *Landsc. Ecol. Eng.* **2022**, *18*, 351–366. [CrossRef]
- Zhai, T.; Wang, J.; Fang, Y.; Qin, Y.; Huang, L.; Chen, Y. Assessing Ecological Risks Caused by Human Activities in Rapid Urbanization Coastal Areas: Towards an Integrated Approach to Determining Key Areas of Terrestrial-Oceanic Ecosystems Preservation and Restoration. *Sci. Total Environ.* **2020**, *708*, 135153. [CrossRef]
- Zhao, Q.; Pepe, A.; Devlin, A.; Zhang, S.; Falabella, F.; Zeni, G.; Wang, Q.; Ding, J.; Dong, D.; Liu, M. Impact of Sea-Level-Rise and Human Activities in Coastal Regions: An Overview. *J. Geod. Geoinf. Sci.* **2021**, *4*, 124.
- Hzami, A.; Heggy, E.; Amrouni, O.; Mahé, G.; Maanan, M.; Abdeljaouad, S. Alarming Coastal Vulnerability of the Deltaic and Sandy Beaches of North Africa. *Sci. Rep.* **2021**, *11*, 2320. [CrossRef]
- Pal, I.; Kumar, A.; Mukhopadhyay, A. Risks to Coastal Critical Infrastructure from Climate Change. *Annu. Rev. Environ. Resour.* **2023**, *48*, 681–712. [CrossRef]
- Environment, U.N. Coastal Zone Management | UNEP—UN Environment Programme. Available online: <https://www.unep.org/topics/ocean-seas-and-coasts/regional-seas-programme/coastal-zone-management> (accessed on 25 November 2024).
- Giardino, A.; Santinelli, G.; Vuik, V. Coastal State Indicators to Assess the Morphological Development of the Holland Coast Due to Natural and Anthropogenic Pressure Factors. *Ocean Coast. Manag.* **2014**, *87*, 93–101. [CrossRef]
- Newton, A.; Icely, J.; Cristina, S.; Perillo, G.M.E.; Turner, R.E.; Ashan, D.; Cragg, S.; Luo, Y.; Tu, C.; Li, Y.; et al. Anthropogenic, Direct Pressures on Coastal Wetlands. *Front. Ecol. Evol.* **2020**, *8*, 144. [CrossRef]
- Wu, W.; Wan, L. 13—Coastal Ecological and Environmental Management under Multiple Anthropogenic Pressures: A Review of Theory and Evaluation Methods. In *Current Trends in Estuarine and Coastal Dynamics*; Wang, X.H., Qiao, L., Mitchell, S., Elliott, M., Eds.; Estuarine and Coastal Sciences Series; Elsevier: Amsterdam, The Netherlands, 2024; Volume 4, pp. 385–415, ISBN 978-0-443-21728-9.
- Griggs, G.; Reguero, B.G. Coastal Adaptation to Climate Change and Sea-Level Rise. *Water* **2021**, *13*, 2151. [CrossRef]
- Hinkel, J.; Lincke, D.; Vafeidis, A.T.; Perrette, M.; Nicholls, R.J.; Tol, R.S.J.; Marzeion, B.; Fettweis, X.; Ionescu, C.; Levermann, A. Coastal Flood Damage and Adaptation Costs under 21st Century Sea-Level Rise. *Proc. Natl. Acad. Sci. USA* **2014**, *111*, 3292–3297. [CrossRef] [PubMed]
- Nazarnia, H.; Nazarnia, M.; Sarmasti, H.; Wills, W.O. A Systematic Review of Civil and Environmental Infrastructures for Coastal Adaptation to Sea Level Rise. *Civ. Eng. J.* **2020**, *6*, 1375–1399. [CrossRef]
- Xu, L.; Cui, S.; Wang, X.; Tang, J.; Nitivattananon, V.; Ding, S.; Nguyen Nguyen, M. Dynamic Risk of Coastal Flood and Driving Factors: Integrating Local Sea Level Rise and Spatially Explicit Urban Growth. *J. Clean. Prod.* **2021**, *321*, 129039. [CrossRef]
- Archetti, R.; Damiani, L.; Bianchini, A.; Romagnoli, C.; Abbiati, M.; Addona, F.; Airoidi, L.; Cantelli, L.; Gaeta, M.G.; Guerrero, M.; et al. Innovative Strategies, Monitoring and Analysis of the Coastal Erosion Risk: The STIMARE Project. In Proceedings of the 29th International Ocean and Polar Engineering Conference, Honolulu, HI, USA, 16–21 June 2019.
- Azevedo de Almeida, B.; Mostafavi, A. Resilience of Infrastructure Systems to Sea-Level Rise in Coastal Areas: Impacts, Adaptation Measures, and Implementation Challenges. *Sustainability* **2016**, *8*, 1115. [CrossRef]
- Bacopoulos, P.; Clark, R.R. Coastal Erosion and Structural Damage Due to Four Consecutive-Year Major Hurricanes: Beach Projects Afford Resilience and Coastal Protection. *Ocean Coast. Manag.* **2021**, *209*, 105643. [CrossRef]
- Scala, P.; Manno, G.; Ciraolo, G. Coastal Dynamics Analyzer (CDA): A QGIS Plugin for Transect Based Analysis of Coastal Erosion. *SoftwareX* **2024**, *28*, 101894. [CrossRef]
- Coelho, C.; Narra, P.; Marinho, B.; Lima, M. Coastal Management Software to Support the Decision-Makers to Mitigate Coastal Erosion. *J. Mar. Sci. Eng.* **2020**, *8*, 37. [CrossRef]
- Coelho, C.; Veloso-Gomes, F.; Silva, R. Shoreline Coastal Evolution Model: Two Portuguese Case Studies. In *Coastal Engineering 2006: (In 5 Volumes)*; World Scientific: Singapore, 2007; pp. 3430–3441.

25. Nativí-Merchán, S.; Caiza-Quinga, R.; Saltos-Andrade, I.; Martillo-Bustamante, C.; Andrade-García, G.; Quiñonez, M.; Cervantes, E.; Cedeño, J. Coastal Erosion Assessment Using Remote Sensing and Computational Numerical Model. Case of Study: Libertador Bolivar, Ecuador. *Ocean Coast. Manag.* **2021**, *214*, 105894. [[CrossRef](#)]
26. Pombo, R.; Fernández-Fernández, S.; Baptista, P.; Coelho, C.; Bernardes, C. Old Forecasts vs Actual Shoreline Evolution: Assessing Model's Performance and Projections Accuracy. *Coast. Eng.* **2022**, *175*, 104143. [[CrossRef](#)]
27. Le Xuan, T.; Ba, H.T.; Thanh, V.Q.; Wright, D.P.; Hasan Tanim, A.; Tran Anh, D. Evaluation of Coastal Protection Strategies and Proposing Multiple Lines of Defense under Climate Change in the Mekong Delta for Sustainable Shoreline Protection. *Ocean Coast. Manag.* **2022**, *228*, 106301. [[CrossRef](#)]
28. Lima, M.; Coelho, C.; Veloso-Gomes, F.; Roebeling, P. An Integrated Physical and Cost-Benefit Approach to Assess Groins as a Coastal Erosion Mitigation Strategy. *Coast. Eng.* **2020**, *156*, 103614. [[CrossRef](#)]
29. Nordstrom, K.F. Living with Shore Protection Structures: A Review. *Estuar. Coast. Shelf Sci.* **2014**, *150*, 11–23. [[CrossRef](#)]
30. Zehro, K. Specifications and Types of Seawall Structures Needed to Protect Beaches from Sand Erosion and Storm Disasters. *Int. J. Adv. Eng. Sci. Appl.* **2021**, *2*, 13–18. [[CrossRef](#)]
31. Dean, R.G.; Dalrymple, R.A. *Coastal Processes with Engineering Applications*; Cambridge University Press: Cambridge, UK, 2004; ISBN 978-0-521-60275-4.
32. Hanson, H.; Kraus, N.C.; Nakashima, L.D. *Shoreline Change behind Transmissive Detached Breakwaters*; American Society of Civil Engineers: Reston, VA, USA, 1989; Volume 1, pp. 568–582. Available online: https://repository.tudelft.nl/file/File_e3c5f47b-7b59-4bc0-878a-73a0b000421a?preview=1#page=44 (accessed on 31 August 2024).
33. Hanson, H.; Brampton, A.; Capobianco, M.; Dette, H.H.; Hamm, L.; Laustrup, C.; Lechuga, A.; Spanhoff, R. Beach Nourishment Projects, Practices, and Objectives—A European Overview. *Coast. Eng.* **2002**, *47*, 81–111. [[CrossRef](#)]
34. Luo, S.; Liu, Y.; Jin, R.; Zhang, J.; Wei, W. A Guide to Coastal Management: Benefits and Lessons Learned of Beach Nourishment Practices in China over the Past Two Decades. *Ocean Coast. Manag.* **2016**, *134*, 207–215. [[CrossRef](#)]
35. Pinto, C.A.; Silveira, T.M.; Teixeira, S.B. Beach Nourishment Practice in Mainland Portugal (1950–2017): Overview and Retrospective. *Ocean Coast. Manag.* **2020**, *192*, 105211. [[CrossRef](#)]
36. Cantasano, N.; Boccalaro, F.; Ietto, F. Assessing of Detached Breakwaters and Beach Nourishment Environmental Impacts in Italy: A Review. *Environ. Monit. Assess.* **2022**, *195*, 127. [[CrossRef](#)]
37. Dong, W.S.; Ariffin, E.H.; Saengsupavanich, C.; Rashid, M.A.M.; Shukri, M.H.M.; Ramli, M.Z.; Miskon, M.F.; Jeofry, M.H.; Yunus, K.; Ghazali, N.H.M. Adaptation of Coastal Defence Structure as a Mechanism to Alleviate Coastal Erosion in Monsoon Dominated Coast of Peninsular Malaysia. *J. Environ. Manag.* **2023**, *333*, 117391. [[CrossRef](#)]
38. Dong, X.; Zhang, Z.; Fang, K.; Yi, F. The Evolution of Nourished Beach Profile with Permeable Submerged Breakwater in a Wave Flume. In Proceedings of the 32nd International Ocean and Polar Engineering Conference, Shanghai, China, 5 June 2022.
39. Ruol, P.; Martinelli, L.; Favaretto, C.; Scroccaro, D. Innovative Sand Groin Beach Nourishment with Environmental, Protective, and Recreational Purposes. *Int. J. Offshore Polar Eng.* **2020**, *30*, 364–374. [[CrossRef](#)]
40. Zimmerman, T.; Miller, J.K. UAS-SfM Approach to Evaluate the Performance of Notched Groins within a Groin Field and Their Impact on the Morphological Evolution of a Beach Nourishment. *Coast. Eng.* **2021**, *170*, 103997. [[CrossRef](#)]
41. Afentoulis, V.; Papadimitriou, A.; Belibassakis, K.; Tsoukala, V. A Coupled Model for Sediment Transport Dynamics and Prediction of Seabed Morphology with Application to 1DH/2DH Coastal Engineering Problems. *Oceanologia* **2022**, *64*, 514–534. [[CrossRef](#)]
42. Alvarez-Cuesta, M.; Toimil, A.; Losada, I.J. Modelling Long-Term Shoreline Evolution in Highly Anthropized Coastal Areas. Part 1: Model Description and Validation. *Coast. Eng.* **2021**, *169*, 103960. [[CrossRef](#)]
43. Dang, B.-L.; Nguyen-Xuan, H.; Abdel Wahab, M. Numerical Study on Wave Forces and Overtopping over Various Seawall Structures Using Advanced SPH-Based Method. *Eng. Struct.* **2021**, *226*, 111349. [[CrossRef](#)]
44. Foti, E.; Musumeci, R.E.; Stagnitti, M. Coastal Defence Techniques and Climate Change: A Review. *Rendiconti Lincei Sci. Fis. E Nat.* **2020**, *31*, 123–138. [[CrossRef](#)]
45. LeMéhauté, B.; Soldate, M. *Mathematical Modeling of Shoreline Evolution*; U.S. Army, Corps of Engineers, Coastal Engineering Research Center: New York, NY, USA, 1977.
46. Manilam, S.; Pochai, N. A Non-Dimensional Mathematical Model of Shoreline Evolution with a Groin Structure Using an Unconditionally Stable Explicit Finite Difference Technique. *IAENG Int. J. Appl. Math.* **2022**, *52*, 1–9.
47. Nguyen, N.-M.; Van, D.D.; Le, D.T.; Cong, S.D.; Chuong, L.T.; Hai, T.D.; Nguyen, T.C.; Wright, D.; Tanim, A.H.; Pham, N.T.; et al. Experimental and Numerical Modeling of Pile-Rock Breakwater Gap Arrangement for Optimal Coastal Erosion Protection in Deltaic Coasts. *Ocean Eng.* **2023**, *280*, 114625. [[CrossRef](#)]
48. Roelvink, D.; Huisman, B.; Elghandour, A.; Ghonim, M.; Reyns, J. Efficient Modeling of Complex Sandy Coastal Evolution at Monthly to Century Time Scales. *Front. Mar. Sci.* **2020**, *7*, 535. [[CrossRef](#)]
49. Tsiaras, A.-C.; Karambas, T.; Koutsouvela, D. Design of Detached Emerged and Submerged Breakwaters for Coastal Protection: Development and Application of an Advanced Numerical Model. *J. Waterw. Port Coast. Ocean Eng.* **2020**, *146*, 04020012. [[CrossRef](#)]

50. Unyapoti, P.; Pochai, N. A Shoreline Evolution Model With the Wavelength Effect of Breaking Waves on Groin Structures. *IAENG Int. J. Comput. Sci.* **2022**, *49*, 683–694.
51. Hunt, E.; Davidson, M.; Steele, E.C.C.; Amies, J.D.; Scott, T.; Russell, P. Shoreline Modelling on Timescales of Days to Decades. *Camb. Prisms Coast. Futures* **2023**, *1*, e16. [[CrossRef](#)]
52. Lesser, G.R.; Roelvink, J.A.; van Kester, J.A.T.M.; Stelling, G.S. Development and Validation of a Three-Dimensional Morphological Model. *Coast. Eng.* **2004**, *51*, 883–915. [[CrossRef](#)]
53. Pelnard-Considère, R. Essai de théorie de l'évolution des formes de rivage en plages de sable et de galets. *Journ. L'Hydraul.* **1957**, *4*, 289–298.
54. Roelvink, D.; Reniers, A.; van Dongeren, A.; van Thiel de Vries, J.; McCall, R.; Lescinski, J. Modelling Storm Impacts on Beaches, Dunes and Barrier Islands. *Coast. Eng.* **2009**, *56*, 1133–1152. [[CrossRef](#)]
55. Thieler, E.R.; Orrin, H.P., Jr.; Young, R.S.; Bush, D.M.; Chai, F. The Use of Mathematical Models to Predict Beach Behavior for U.S. Coastal Engineering: A Critical Review. *J. Coast. Res.* **2000**, *16*, 48–70.
56. Armono, H.D.; Citrosiswoyo, W.; Muzaki, F.K. Shoreline Change Model after Artificial Reefs Deployment in Tlangoh, Bangkalan, Madura. *BIO Web Conf.* **2024**, *89*, 09002. [[CrossRef](#)]
57. Ülger, M.; Tanrivermiş, Y. Prevention of the Effects of Coastal Structures on Shoreline Change Using Numerical Modeling. *Ocean Coast. Manag.* **2023**, *243*, 106752. [[CrossRef](#)]
58. Hanson, H.; Kraus, N.C. Long-Term Evolution of a Long-Term Evolution Model. *J. Coast. Res.* **2011**, *59*, 118–129. [[CrossRef](#)]
59. Huang, Y.-L. Applications of GENESIS on Modeling Structure-Induced Shoreline Changes. 2005. Available online: <https://agris.fao.org/search/en/providers/122415/records/6473682c08fd68d54605d499> (accessed on 31 August 2024).
60. Tomasichio, G.R.; Francone, A.; Simmonds, D.J.; D'Alessandro, F.; Frega, F. Prediction of Shoreline Evolution. Reliability of a General Model for the Mixed Beach Case. *J. Mar. Sci. Eng.* **2020**, *8*, 361. [[CrossRef](#)]
61. Splinter, K.D.; Coco, G. Challenges and Opportunities in Coastal Shoreline Prediction. *Front. Mar. Sci.* **2021**, *8*, 788657. [[CrossRef](#)]
62. Wise, R.A.; Smith, S.; Larson, M. SBEACH: Numerical Model for Simulating Storm-Induced Beach Change. Report 4. Cross-Shore Transport under Random Waves and Model Validation with SUPERTANK and Field Data. 1997. Available online: <https://citeseerx.ist.psu.edu/document?repid=rep1&type=pdf&doi=46738c357123e6cb52c3b5b81871b160be17a3d5> (accessed on 31 August 2024).
63. Robinet, A.; Idier, D.; Castelle, B.; Mariieu, V. A Reduced-Complexity Shoreline Change Model Combining Longshore and Cross-Shore Processes: The LX-Shore Model. *Environ. Model. Softw.* **2018**, *109*, 1–16. [[CrossRef](#)]
64. Barnard, P.L.; van Ormondt, M.; Erikson, L.H.; Eshleman, J.; Hapke, C.; Ruggiero, P.; Adams, P.N.; Foxgrover, A.C. Development of the Coastal Storm Modeling System (CoSMoS) for Predicting the Impact of Storms on High-Energy, Active-Margin Coasts. *Nat. Hazards* **2014**, *74*, 1095–1125. [[CrossRef](#)]
65. Bayram, A.; Larson, M.; Hanson, H. A New Formula for the Total Longshore Sediment Transport Rate. *Coast. Eng.* **2007**, *54*, 700–710. [[CrossRef](#)]
66. Hoagland, S.W.H.; Irish, J.L.; Weiss, R. Morphodynamic and Modeling Insights from Global Sensitivity Analysis of a Barrier Island Evolution Model. *Geomorphology* **2024**, *451*, 109087. [[CrossRef](#)]
67. Vitousek, S.; Barnard, P.L.; Limber, P.; Erikson, L.; Cole, B. A Model Integrating Longshore and Cross-shore Processes for Predicting Long-term Shoreline Response to Climate Change. *J. Geophys. Res. Earth Surf.* **2017**, *122*, 782–806. [[CrossRef](#)]
68. Frey, A.E.; Connell, K.J.; Hanson, H.; Larson, M.; Thomas, R.C.; Munger, S.; Zundel, A. GenCade Version 1 Model Theory and User's Guide. Available online: https://d1wqtxts1xzle7.cloudfront.net/108472042/a576160-libre.pdf?1701900462=&response-content-disposition=inline;+filename=GenCade_version_1_model_theory_and_user.pdf&Expires=1737085937&Signature=G6lNvvG-36ByCTzlt7j48QHjriqooki7ywVS1RTYnmWvdqg9apWKDoQez4uZXXH9r3RKUHSyLL2MSg7ghOGDVNe0ZFKpDxlgzJhb6CoBz50B~SqwVsFhhCcVnd4jcG8yECfdgodyvLjoahc8syMs2e7OceXo8pW5AFJSVqpobIU23X4DSxd3FeYzmLIV5lq0cVzDOGZ6jMzeBQePUnAGZB7BxBwBndYOPthwfqjFaOWjS01QAzoim9RjwvBs8BmElaOp1yaXI9dn-WwWrWTRa1L07aXBOsxLnj8aPANijWqKNjNDJ8BU91D68YXYCCZ5NJW5TOLCFsUHx-zbjoVw__&Key-Pair-Id=APKAJLOHF5GGSLRBV4ZA (accessed on 31 August 2024).
69. Tao, H.-C.; Hsu, T.-W.; Fan, C.-M. An Improved One-Line Evolution Formulation for the Dynamic Shoreline Planforms of Embayed Beaches. *Water* **2024**, *16*, 774. [[CrossRef](#)]
70. Camus, P.; Mendez, F.; Medina, R.; Tomas, A.; Izaguirre, C. High Resolution Downscaled Ocean Waves (DOW) Reanalysis in Coastal Areas. *Coast. Eng.* **2013**, *72*, 56–68. [[CrossRef](#)]
71. Valsamidis, A.; Reeve, D.E. A New Approach to Analytical Modelling of Groyne Fields. *Cont. Shelf Res.* **2020**, *211*, 104288. [[CrossRef](#)]
72. Petti, M. *Fondamenti Di Idraulica Marittima e Costiera*; Forum: Udine, Italy, 2021; ISBN 978-88-3283-2747-7.
73. Bosboom, J.; Stive, M.J.F. *Coastal Dynamics*; TU Delft Open: Delft, The Netherlands, 2023; ISBN 978-94-6366-370-0. [[CrossRef](#)]
74. Kamphuis, J. Physical Modelling of Coastal Processes. *Adv. Coast. Ocean Eng.* **1996**, *2*, 79–114.
75. Kamphuis, J.W. *Introduction to Coastal Engineering and Management*; World Scientific: Singapore, 2000; Volume 6.

76. Dean, R.G. Relative Validities of Water Wave Theories. *J. Waterw. Harb. Coast. Eng. Div.* **1970**, *96*, 105–119. [CrossRef]
77. Mil-Homens, J.; Ranasinghe, R.; van Thiel de Vries, J.S.M.; Stive, M.J.F. Re-Evaluation and Improvement of Three Commonly Used Bulk Longshore Sediment Transport Formulas. *Coast. Eng.* **2013**, *75*, 29–39. [CrossRef]
78. Smith, E.R.; Wang, P.; Zhang, J. Evaluation of the CERC Formula Using Large-Scale Laboratory Data. Available online: https://digitalcommons.usf.edu/gly_facpub/238/ (accessed on 31 August 2024).
79. Miller, J.K.; Dean, R.G. A Simple New Shoreline Change Model. *Coast. Eng.* **2004**, *51*, 531–556. [CrossRef]
80. Silvester, R.; Hsu, J.R.C. *Coastal Stabilization. Advanced Series on Ocean Engineering*; World Scientific: Singapore, 1997; Volume 14.
81. Hsu, R.J.; Lee, J.L.; Klein, A.H.D.F.; Gonzalez, M.; Medina, R. *Headland-Bay Beaches: Static Equilibrium Concept For Shoreline Management*; World Scientific: Singapore, 2021; ISBN 9789811227738.
82. Reeve, D.E.; Valsamidis, A. On the Stability of a Class of Shoreline Planform Models. *Coast. Eng.* **2014**, *91*, 76–83. [CrossRef]
83. Zacharioudaki, A.; Reeve, D.E. Semianalytical Solutions of Shoreline Response to Time-Varying Wave Conditions | Journal of Waterway, Port, Coastal, and Ocean Engineering | Vol 134, No 5. Available online: [https://ascelibrary.org/doi/abs/10.1061/\(ASCE\)0733-950X\(2008\)134:5\(265\)](https://ascelibrary.org/doi/abs/10.1061/(ASCE)0733-950X(2008)134:5(265)) (accessed on 31 August 2024).
84. Scala, P.; Manno, G.; Ciraolo, G. Semantic Segmentation of Coastal Aerial/Satellite Images Using Deep Learning Techniques: An Application to Coastline Detection. *Comput. Geosci.* **2024**, *192*, 105704. [CrossRef]
85. Baptista, P.; Coelho, C.; Pereira, C.; Bernardes, C.; Veloso-Gomes, F. Beach Morphology and Shoreline Evolution: Monitoring and Modelling Medium-Term Responses (Portuguese NW Coast Study Site). *Coast. Eng.* **2014**, *84*, 23–37. [CrossRef]

Disclaimer/Publisher’s Note: The statements, opinions and data contained in all publications are solely those of the individual author(s) and contributor(s) and not of MDPI and/or the editor(s). MDPI and/or the editor(s) disclaim responsibility for any injury to people or property resulting from any ideas, methods, instructions or products referred to in the content.